Oligodendrocyte Death in Pelizaeus-Merzbacher Disease is Rescued by Iron Chelation

Hiroko Nobuta[1], Nan Yang[4], Yi-Han Ng[4], Samuele Marro[4], Khalida Sabeur[1], Manideep Chavali[1], John Stockley[11,12], David W. Killilea[6], Patrick Walter[7], Chao Zhao[10], Philip Huie Jr.[8], Steven A. Goldman[9], Arnold Kriegstein[1,3], Robin J.M. Franklin[10,12], David Rowitch[1,2,10,11,12^], Marius Wernig[4,5^]

[1]Eli and Edythe Broad Center of Regeneration Medicine and Stem Cell Research, Departments of Pediatrics, [2]Neurosurgery, [3]Neurology, University of California San Francisco, San Francisco, CA 94143, USA; [4]Institute for Stem Cell Biology and Regenerative Medicine, [5]Department of Pathology, Stanford University School of Medicine, Stanford, CA 94305, USA; [6]Children's Hospital Oakland Research Institute, Oakland, CA 94609, USA; [7]Department of Biology, University of Victoria, British Columbia, Canada; [8]Department of Surgical Pathology, Stanford Health Care, Palo Alto, CA 94305, USA; [9]Department of Neurosurgery, University of Rochester Medical Center, Rochester, NY 14642, USA; [10]Departments of Clinical Neurosciences and [11]Paediatrics, [12]Wellcome Trust-Medical Research Council Cambridge Stem Cell Institute, University of Cambridge, Hills Road, Cambridge, UK.

^Corresponding authors: Marius Wernig: wernig@stanford.edu; David Rowitch: dhr25@medschl.cam.ac.uk

Lead contacts: Marius Wernig: wernig@stanford.edu; David Rowitch: dhr25@medschl.cam.ac.uk

The authors have declared that no conflict of interest exists.

Running title: Iron Chelation Promotes Oligodendrocyte Survival in PMD

Keywords: Leukodystrophy, patient models, iron chelation, oligodendrocyte, myelination, induced pluripotent stem cells, gene correction, ferroptosis

SUMMARY

Pelizaeus-Merzbacher disease (PMD) is a X-linked leukodystrophy caused by mutations in *Proteolipid Protein 1 (PLP1),* encoding a major myelin protein, resulting in profound developmental delay and early lethality. Previous work showed involvement of unfolded protein response (UPR) and endoplasmic reticulum (ER) stress pathways, but poor *PLP1* genotype-phenotype associations in patients suggest additional pathogenetic mechanisms. Using induced pluripotent stem cell (iPSC) reprogramming and gene-correction, we here show that PMD patient-derived oligodendrocytes can develop to the pre-myelinating stage, but subsequently undergo cell death. Activation of UPR and ER stress pathways occurred variably among patient-specific lines carrying different *PLP1* mutations. Instead, mutant oligodendrocytes demonstrated key hallmarks of ferroptosis including lipid peroxidation, abnormal iron metabolism and hypersensitivity to free iron. Iron chelation rescued mutant oligodendrocyte apoptosis, survival and differentiation *in vitro*, and post-transplantation *in vivo*. Moreover, systemic treatment of *Plp1*-mutant *Jimpy* mice with deferiprone, a small molecule iron chelator, reduced oligodendrocyte apoptosis and enabled myelin formation. Thus, oligodendrocyte iron-induced cell death and myelination is rescued by iron chelation in PMD pre-clinical models.

INTRODUCTION

Pelizaeus-Merzbacher disease (PMD) is a congenital X-linked recessive leukodystrophy caused by mutations in the *Proteolipid Protein 1 (PLP1)* gene with an incidence of 1:200,000 to 1:500,000 (Hobson and J., 1999). PLP1 is one of the main protein components in myelin of the central nervous system (CNS) and lack of myelination is the main pathological characteristic of the disease. Accordingly, the clinical presentation can show pervasive neuro-developmental delay and generalized low muscle tone. Early-severe (aka connatal) PMD patients show respiratory difficulties and nystagmus at birth and later neurodegeneration and death at early teenage years (Woodward, 2008).

PLP1 mutations comprising gene duplications, and missense point mutations of *PLP1* can result in marked hypomyelination of the CNS (Woodward, 2008). While loss-of-function mutations also can occur, these typically show the mildest phenotypes (Sistermans et al., 1996). How these *PLP1* mutations lead to lack of myelination, however, is not well understood and therefore no curative treatment options are currently available. Studies in mice and tissue culture cells have shown that oligodendrocytes, the myelinating cells of CNS, can be dysfunctional and abnormal Plp1 trafficking in the endoplasmic reticulum (ER) of oligodendrocytes can lead to apoptosis by activation of the unfolded protein response (UPR) (Dhaunchak and Nave, 2007; Elitt et al., 2018; Kramer-Albers et al., 2006). These studies suggest deficiencies in oligodendrocyte survival rather than problems of myelin composition with mutant *PLP1*. The involvement of ER stress and activation of the UPR could be confirmed in human oligodendrocyte cell models which were derived from patients' iPSCs (Nevin et al., 2017; Numasawa-Kuroiwa et al., 2014). Of note, a recent study demonstrated that only a subset of *PLP1* mutations show activation of an UPR in patient iPSC-derived oligodendrocytes (Nevin et al., 2017). Together with the lack of a consistent genotype-phenotype correlation in patients this result suggests the existence of additional pathobiological mechanisms that lead to dysfunctional oligodendrocytes or myelin formation in PMD. Here, we therefore investigated the

cell biological consequences of *PLP1* mutations in greater detail using patient iPSC-derived oligodendrocytes and genetically corrected controls as a model system.

RESULTS

PLP1^{G74E} mutant oligodendrocytes develop but subsequently die and cannot properly differentiate into myelinating cells.

To generate human cellular models of PMD we initially obtained a skin biopsy from a PMD patient with early-severe PMD who presented with nystagmus, respiratory distress, loss of developmental milestones, spasticity and hypomyelination (Gupta et al., 2012). Genotyping revealed a point mutation in *PLP1* gene at G74E (hereafter *PLP1*^{G74E} mutation), which causes a single amino acid change from glycine to glutamic acid in the second transmembrane domain (Fig. 1A,C). We generated patient iPSC lines by episomal reprogramming (Diecke et al., 2015) that showed typical features of pluripotency (expression of OCT4, TRA 1-60 and generation of mature teratomas) and normal karyotype (Supplementary Fig. 1A-C).

To assess potential phenotypic abnormalities in patient-derived oligodendrocyte precursor cells (OPCs), we adapted an established protocol (Supplementary Fig. 2A) (Douvaras and Fossati, 2015). Oligodendrocyte differentiation of these lines evidenced significant clone-to-clone variability (Supplementary Fig. 2B), prompting us to develop line-specific isogenic controls for this study. To that end, we corrected the *PLP1* ^{G74E} mutation in this patient's iPSCs using adeno-associated virus-mediated homologous recombination (Supplementary Fig. 2D). Reassuringly, PMD mutant and gene-corrected iPSCs now showed similar differentiation dynamics as determined by appearance of neural rosettes and *SOX1*, *PAX6*, *NKX2.2*, *OLIG2*, and *PLP1* expressing cells (Supplementary Fig. 2E) and reduced variability in oligodendrocyte generation within subclones (clonal lines obtained from single colonies after gene-correction of a parental clone) (Supplementary Fig. 2C). Expression of O4, a marker of oligodendrocytes at a pre-myelinating stage with immature morphology, first appeared around day 35 (D35) in both

mutant and corrected cells and increased subsequently (Supplementary Fig. 2F). Although on D45 numbers of mutant and corrected $O4^+$ cells were similar (Fig. 1D-E,H), by D55 we observed significant losses of $O4^+$ mutant cells compared to isogenic controls (Fig. 1F-G, H, Supplementary Fig. 2G). The onset of this phenotype was accompanied by induction of the mutant PLP1 protein in mutant cells at around D45 (Supplementary Fig. 2F). Remaining $O4^+$ mutant cells failed to differentiate into MBP+ cells with mature and ramified oligodendrocyte morphology (Fig. 1K-P) and did not acquire robust expression of the mature marker myelin basic protein (MBP) (Fig. 1F-G, I). While we found about twice as many Caspase-3 positive mutant cells on D55, indicating apoptosis, this mechanism alone did not account for the observed 5-fold levels of cell attrition, and suggested additional mechanisms of cell death (Fig. 1J, Supplementary Fig. 2H).

Next, we sought to test the myelination capacity of human PMD mutant and gene-corrected OPCs. When plated on previously established human fetal brain slice explant cultures (Fig. 2A see Methods) (Hansen et al., 2010) and analyzed at the limit of culture duration (3 weeks), mutant cells failed to acquire mature oligodendrocyte morphology or expressed minimal level of MBP, contrasting the gene-corrected cells (Fig. 2, B-D). We then transplanted mutant and corrected OPCs into the brains of immunocompromised *Shiverer* (*Shi)* mice, which lack compact myelin due to disruption of the *Mbp* gene and die at around 16 weeks of age (Roach et al., 1983). We purified iPSC-derived OPCs by $O4^+$ antibody-based immunopanning (Harrington et al., 2010) (Fig. 2E) and transplanted them into the cerebellum of *Shi* mice at postnatal day (P) 1. Unlike mutant cells, 13 weeks post-transplantation near animal's death, corrected human OPCs migrated from the injection site and differentiated into robustly MBP^+ oligodendrocytes that exhibited a typical morphology with membrane ensheathment of multiple axons (Fig. 2F,H; Mean MBP+/human specific marker+ cells per unit area: mutant 0.875 ± 0.295, corrected 8.125 ± 0.990, t-test p = 0.0003). Electron microscopic analysis showed restoration of compact myelin in areas transplanted with corrected cells (G-ratio 0.8453 ± 0.02878), but not with mutant (G-

ratio 0.9238 ± 0.00975, t-test p = 0.0039) (Fig. 2I-J). In contrast, most mutant cells even failed to survive in the host brain (Fig. 2G). Thus, the *PLP1*^{G74E} mutation rendered oligodendrocytes unable to survive or achieve terminal differentiation *in vitro,* in explant slices *ex vivo* or in mouse brain *in vivo*.

Lack of ER stress and unfolded protein response in *PLP1*^{G74E} mutant cells.

ER stress and activation of the UPR pathway leading to apoptosis is implicated for *PLP1* mutations in mouse models (Dhaunchak and Nave, 2007; Elitt et al., 2018; Kramer-Albers et al., 2006; Numasawa-Kuroiwa et al., 2014; Southwood et al., 2002) (but also see (Nevin et al., 2017)). Because conventional apoptosis could only partially explain observed cell death (see above), we next investigated the underlying mechanisms of the survival and differentiation deficiency of PMD mutant cells. Surprisingly, we found that UPR/ER stress pathway genes were not activated in purified human O4^{+} cells from the *PLP1*^{G74E} mutant oligodendrocytes (Fig. 3A). We also did not observe accumulation of the *PLP1*^{G74E} mutant protein in the ER, instead found it extensively dispersed from the ER into the fine processes of the cell (Fig. 3C,E, G-L). We could find only rare examples of mutant PLP1 protein that co-localized with the ER marker KDEL (Fig. 3B,D, F), indicating ER retention was minimal. We tested inhibitors of the ER stress pathways but these did not rescue survival *PLP1*^{G74E} mutant oligodendrocytes in culture (Supplementary Fig. 3A). Finally, transplanted mutant OPCs did not express the ER stress marker CHOP protein *in vivo* (Supplementary Fig. 3B). Together, these findings indicated that cell death of *PLP1*^{G74E} mutant OPCs did not involve significant UPR or ER stress pathway activation, and suggested additional pathobiological pathways.

Accumulation of oxidative species and activation of oxidative stress genes in *PLP1*^{G74E} mutant oligodendrocytes.

Oxidative stress is a common pathogenetic mechanism in many neurological disorders. Indeed, purified *PLP1*^{G74E} mutant OPCs showed strong induction of several oxidative stress marker genes when compared to gene-corrected OPCs (Fig. 3M). Moreover, mutant cultures more strongly labeled with CellROX, a dye that detects reactive oxygen species (ROS) in live cells, compared to gene-corrected cultures, and a higher fraction of mutant OPCs was labeled with the dye (Fig. 3N-P). We conclude that the *PLP1*^{G74E} mutation induced high oxidation levels in OPCs. The potential causes of increased oxidation are manifold and we therefore continued to search for additional pathological abnormalities in mutant cells.

Marked deregulation of iron metabolism in human *PLP1*^{G74E} mutant oligodendrocytes

Rodent oligodendrocytes express high levels of transferrin (TF) (Espinosa de los Monteros et al., 1999; Leitner and Connor, 2012; Zhang et al., 2014), the major iron transporter for intracellular uptake of iron (Brissot and Loreal, 2016; Hentze et al., 2010). We confirmed similar findings in human cells, relatively high TF expression in primary fetal human O4+ oligodendrocytes (Fig. 4A-D) compared to other neural cells (Fig. 4E) and increased levels of oxidative stress genes (Fig. 4F). Dysregulation in iron metabolism can pose oxidative stress for which oligodendrocytes are particularly vulnerable (Back et al., 1998; Butts et al., 2008; Khorchid et al., 2002). We therefore investigated whether iron metabolism was dysregulated in PMD mutant cells. Expression profiling showed several iron regulation genes were indeed significantly de-regulated including transferrin itself (Fig. 4I). To further corroborate these findings, we performed quantitative immunoblotting of some key iron regulatory proteins. *PLP1*^{G74E} mutant OPCs showed a consistent downregulation of TF (iron transporter) and ferritin (iron storage), and up-regulation of the iron regulatory protein 1 (IRP1) (Fig. 4J). Flow cytometric analysis of mutant and corrected oligodendrocytes revealed about a two-fold upregulation of the transferrin receptor (Fig. 4G-H, Supplementary Fig. 4A).

Human *PLP1*^{G74E} mutant oligodendrocytes exhibit hallmarks of ferroptosis: iron-toxicity and lipid-peroxidation.

Having observed a dysregulation of key iron metabolism regulatory proteins, we sought to explore potential functional consequences of these expression changes. To investigate the role of TF and free iron, we differentiated mutant and corrected iPSCs without additional TF, with addition of (iron-free) apo-transferrin (TF) or (iron-bound) holo-TF from days 35 to 55. This is the time frame in which mutant oligodendrocyte cell death begins and PLP1 protein expression is initiated (Supplementary Fig. 2F). Remarkably, addition of apo-TF to the media completely restored mutant oligodendrocytes' viability to the level of genetic rescue (Fig. 5A-F,K). Apo-TF is a central extracellular iron transporter and has high affinity for free iron; thus, it effectively reduces free extracellular iron concentration as a chelator while making it available to cells as holo-TF via TF receptors. Because addition of holo-TF did not have beneficial effects (Fig. 5C-D,K) we deduced that the rescue is caused by the effective decrease of the extracellular iron concentration rather than making more iron available to cells. This conclusion is corroborated by our observation that the two FDA-approved small molecule iron chelators deferoxamine (DFO) and deferiprone (DFP) rescued mutant cells just as Apo-TF treatment did (Fig. 5G-H,K Supplementary Fig. 4B-C). Elevating the extracellular iron concentration reversed effects of apo-TF in mutant cells suggesting an iron-specific effect (Fig. 5I-K). Indeed, no other divalent transition metal ions tested led to increased apoptosis or halted differentiation in mutant or corrected oligodendrocytes (Fig. 5L-M). We further found that Apo-TF, DFO, or DFP treatment normalized the overall number of $O4^+$ cells, apoptosis, and differentiation into MBP^+ cells (Supplementary Fig. 4B-E). Of note, Apo-TF treatment had no significant effect on gene-corrected control oligodendrocytes suggesting that the *PLP1*^{G74E} mutation increased the sensitivity to iron in oligodendrocytes (Fig. 5F,K).

Iron-mediated cell death can be due to ferroptosis, which comprises iron-toxicity and iron-dependent lipid peroxidation (Dixon et al., 2012). We found that *PLP1*^{G74E} mutant

oligodendrocytes undergo increased oxidative stress and discovered that iron chelation normalizes ROX, an oxidation-sensitive dye in live cells (Supplementary Fig. 4F). To more specifically assess whether cells undergo lipid peroxidation, we optimized an assay for accumulation of lipid ROS for our oligodendrocyte cultures (Naguib, 1998). Indeed, *PLP1*^{G74E} mutant cultures showed both general and oligodendrocyte-specific increase in lipid ROS, suggesting peroxidization of cellular lipids during differentiation (Fig. 5N-P). We noted that not all mutant cells showed accumulation of lipid ROS (<60% of O4+ cells), and together with the evidence for Caspase-3 dependent apoptotic cell death in about 40% of O4+ cells (Fig. 1J), we conclude that multiple modes of cell death were at work. Further studies are needed to confirm that lipid ROS production lies downstream of iron induced toxicity in oligodendrocytes affected by PMD that are rescued by chelation.

As shown (Fig. 5P), addition of Apo-TF and DFO reduced lipid ROS^{+} cells to wild type levels indicating that lipid peroxidation was iron-dependent. We next used a series of lipophilic and hydrophilic antioxidants to assess whether the lipid ROS is responsible for the mutant oligodendrocyte phenotype. Compared to hydrophilic antioxidants GSH and NAC, lipophilic antioxidants BHT and Trolox rescued oligodendrocyte differentiation and/or apoptosis (Fig. 5Q-R Supplementary Fig. 4G), supporting lipid ROS as the key inducer of mutant oligodendrocyte death. These findings indicate that the *PLP1*^{G74E} mutation renders oligodendrocytes more sensitive to extracellular free iron, which leads to elevated lipid peroxidation, block of differentiation and cell death – all key hallmarks of ferroptosis-mediated cell death.

Iron chelation rescues survival and maturation of transplanted human *PLP1*^{G74E} mutant oligodendrocytes in mouse brains and human brain slices.

We next asked whether iron chelation would promote survival and differentiation of human *PLP1*-mutant OPCs *in vivo*. We tested whether O4+ mutant cells, grown in conditions of iron chelation, had enhanced survival and/or myelinating capacity *in vivo*. O4^{+} cells were purified

and transplanted into the cerebellum of immunocompromised *Shi* mice (Fig. 6A). Mutant human OPCs pre-treated with apo-TF or DFO from D35-55 of the differentiation protocol readily engrafted and gave rise to mature MBP^+ cells, in contrast to untreated cells (Mean MBP+/human specific marker+ cells: untreated 0.875 ± 0.295, apo-TF treated 8.80 ± 1.20, DFO treated 8.40 ± 1.470, One-way ANOVA $p < 0.0001$) (Fig. 6B-D). Ultrastructural analysis showed multilayer ensheathment of axons by mutant apo-TF- (G-ratio 0.8318 ± 0.02442, $p = 0.0008$) or DFO-treated (G-ratio 0.8388 ± 0.0155, $p = 0.0013$) but not untreated cells (G-ratio 0.9238 ± 0.009750, One-way ANOVA $p = 0.031$) (Fig. 6E-G). Similarly, when mutant oligodendrocytes were pre-treated with apo-TF or DFO for 7-10 days and then placed on human fetal brain slice cultures, they showed a substantially improved differentiation (Fig. 6H-L). Thus, iron chelator pre-treatment of mutant O4+ OPCs enhanced survival and differentiation in mouse brain *in vivo.*

Iron chelation rescues additional *PLP1* mutations in human and mouse oligodendrocytes.

Our findings with the $PLP1^{G74E}$ mutation raised the question whether iron sensitivity is a more common phenomenon in other *PLP1* PMD-relevant mutations. To address this question we generated OPCs from PMD patients carrying a $PLP1^{T75P}$ point mutation (Gupta et al., 2012), another point mutation $PL1^{F233L}$ resulting in exon 6 deletion (Nevin et al., 2017), and *PLP1* duplication (Nevin et al., 2017). Remarkably, the $PLP1^{T75P}$ point mutation and the duplication, but not the exon 6 mutations were also rescued by the iron chelation (Fig. 7A-G). We also investigated the severe PMD *Jimpy* mouse model that harbors a *Plp1* point mutation that affects the splicing of exon 5 (Dautigny et al., 1986; Sidman et al., 1964). While untreated mutant primary *Jimpy* OPCs *in vitro* showed inhibited differentiation block and nearly universal cell death within 24 hours of growth factor withdrawal (Fig. 7H-I, K-L), 4-day treatment with DFO rescued both parameters to near wild type OPC levels (Fig. 7J-L). These results demonstrate that the ferroptosis-mediated oligodendrocyte death is not restricted to the $PLP1^{G74E}$ mutation

and extends to other *PLP1* mutations. Overall, four out of five *PLP1* mutations tested showed a rescue by iron chelation. Of note, ferroptosis activation is not mutually exclusive with induction of ER stress since the *Jimpy* and other *Plp1* mutations are known to cause a severe UPR activation (Dhaunchak and Nave, 2007; Ikeda et al., 2016; Kramer-Albers et al., 2006).

Systemic treatment of *Jimpy* mice with Deferiprone results in enhanced oligodendrocyte survival and new myelin formation.

The successful rescue of *Jimpy* oligodendrocytes *in vitro* raised the question whether iron chelation may also improve the disease progression *in vivo*. The *Plp1 Jimpy* mutation causes a very aggressive disease; mice do not show any myelin formation, develop severe seizures by postnatal week 3, and die around P28 (Dautigny et al., 1986; Sidman et al., 1964). We systemically administered a blood brain barrier-permeable iron chelator DFP to *Jimpy* mice from P7-14 and P21-28 by i.p. injections (Fig. 7M). A 1-week long interruption (P14-P21) was introduced to prevent anemia (Supplementary Fig. 5D). As shown in Fig. 7N-Q', DFP treatment substantially reduced levels of apoptosis in corpus callosum in *Jimpy* mice (45.63 ± 5.61% reduction from vehicle, t-test p >0.001), and allowed the formation of new myelin in the corpus callosum as determined by electron microscopy at P28. In addition, astrogliosis and microglia activation in the white matter were both reduced (Supplementary Fig. 5E). We also observed a slight improvement of overall animal survival (Supplementary Fig. 5C). Notably, a seven-day course of DFP treatment was sufficient to significantly reduce the UPR/ER stress markers Atf4, phosphorylated Eif2α, and Chop (Elitt et al., 2018) in *Jimpy* OPCs and mature oligodendrocytes *in vivo* (Fig. 7R-W, Supplementary Fig. 5G-J). These findings indicate that ferroptosis-like stress also influences the UPR/ER pathway in *Jimpy*, a severe PMD mutation, and that iron chelation substantially rescues this pathophysiology.

DISCUSSION

Our findings highlight dysregulation of iron metabolism as a significant pathobiological mechanism mediating OPC cell death in severe PMD models. We found evidence for ferroptotic as well as apoptotic cell death mechanisms in PMD oligodendrocytes. Both human and mouse PMD OPCs showed a decrease of transferrin, ferritin, iron export proteins APP and CP, and increased or unchanged IRP1/2 and transferrin receptor expression. While indicating a dysregulated iron metabolic response, the condition of PMD oligodendrocytes is distinct from classic iron overload in hemochromatosis where increased hepatic intracellular iron is associated with high ferritin and ferroportin and low levels of transferrin receptor (Recalcati et al., 2006; Siah et al., 2005). Consistent with ferroptosis, PMD oligodendrocytes exhibited lipid peroxidation and phenotypic rescue by iron chelation (Fig. 5N,P) (Dixon et al., 2012). However, we also found that apoptosis marker Caspase-3 was enriched among some mutant cells and that iron chelation also normalized Caspase-3 levels to control levels (Fig. 5L). Similarly, we observed a reduction of ER stress and apoptosis in *Jimpy* oligodendrocytes rescued by DFO (Fig. 7R-W, Supplmentary Fig. 5G-J). These data suggest that the severe iron sensitivity we observed in PMD oligodendrocytes involve various cell pathogenetic mechanisms of iron-induced ferroptosis, ER stress (Feng and Stockwell, 2018) and apoptosis and that these pathways in some PMD lines are benefitted by chelation. We conclude that mechanisms of Fe-induced cell death in PMD oligodendrocyte are complex, and that further studies are needed to define precise pathway interactions in a patient/mutation-specific manner.

A recent publication described a drug screening platform based on cultured *Jimpy* oligodendrocytes and found the small molecule Ro 25-6981, a N-methyl-D-aspartate (NMDA) receptor antagonist, to enhance survival (Elitt et al., 2018). While the functional target of Ro 25-6981was independent of NMDA receptor, authors showed its modulatory effects on UPR signaling and subsequent increase in myelin in *Jimpy* mice. DFP is a FDA-approved drug

for clinical use in pediatric population thus a viable treatment option for PMD. As shown in *Jimpy* mice, DFP significantly reduced ER stress/UPR markers, suggesting the beneficial effect of DFP in *PLP1* mutations that lead to ER stress/UPR. In contrast, most ER stress/UPR inhibitors (Maly and Papa, 2014) and Ro 25-6981 are not approved for clinical use, and administration of NMDA receptor antagonist (Ro 25-6981) to infant patients whose CNS is still developing may not be ideal.

Unlike gene and cell therapeutic approaches (Gupta et al., 2012), iron chelation aims to support endogenous mutant OPC survival through the "critical window" of transition from pre-myelinating to myelinating stages. Indeed, we found that pre-transplant iron chelation was sufficient to promote survival and myelination of mutant oligodendrocytes in human slice culture and *in vivo* for several months post-transplantation in *Shiverer* mice (Fig. 6A-F). For both slice culture system and *in vivo* transplantation, we characterized the myelin at the limit of the culture duration (3 weeks) or at the end of the lifespan of the *Shiverer* hosts (about14-16 weeks) (Fig. 6A-F, H-L). Up to these points, we observe myelin formation by EM. This suggests that PMD oligodendrocytes are most vulnerable to iron-induced toxicity during dynamic differentiation at the onset of mutant PLP1 expression. While our findings suggest that DFP could be an appropriate therapy for selected PMD patients, it will be important to optimize drug dosage, timing for administration and the long-term benefit to oligodendroglial survival and myelination. Evidence in the literature suggests the involvement of iron pathobiology in multiple sclerosis and neurodegeneration with brain iron accumulation, (Hayflick et al., 2006; Kruer et al., 2010; Stephenson et al., 2014), which suggests our findings might have wider significance beyond PMD.

Acknowledgements

We would like to thank Daniel Morrison for assistance in electron microscopy, Nobuko Uchida for the human-specific STEM121 antibody, Brian Popko for advice on manuscript, Hideyuki

Okano for human PMD iPSC lines. Members of the Wernig and Rowitch laboratories provided advice on experimental design and the manuscript. H.N. acknowledges postdoctoral fellowship support from the European Leukodystrophy Association, and career transition fellowship support from National Multiple Sclerosis Society. M.C. acknowledges funding support from Career Development Grant awarded by Cerebral Palsy Alliance Research Foundation Inc. This work was supported by funding from the National Multiple Sclerosis Foundation (to M.W., D.H. R.), the European Leukodystrophy Association and the New York Stem Cell Foundation (to M.W.), and Action Medical Research, the Adelson Medical Research Foundation, the National Institute for Health Research Cambridge Biomedical Research Centre and the European Research Council (to D.H. R).

Figure Legends

Figure 1. PMD oligodendrocytes die prematurely and fail to differentiate with ramified morphology. A, Three G74E, T75P, and F233L point mutations in *PLP1* described in this paper are located in the second transmembrane domain or extracellular domain. An additional duplication mutation as well as a mouse point mutation (*Jimpy* mouse) were investigated in this study. **B,** Gene targeting strategy to correct the G74E point mutation in exon 3. The targeting vector was cloned into an adeno-associated virus (AAV) vector along with neomycin resistant cassette flanked by loxP sites. Pink bars represent locations for homologous recombination. The neomycin cassette was removed by a transient Cre transfection. **C,** Sanger sequencing validated the accurate correction. **D-E,** On D45, mutant and corrected iPSCs had differentiated to normal-appearing $O4^+$ OPCs. **F-G,** On D55, the mutant cells were fewer, morphologically simpler, and expressed minimum levels of the maturation marker MBP. **H,** Quantification of $O4^+$ cells by flow cytometry on D45 and D55 showed progredient loss of cells (N=3-5, biological replicates). **I,** Immunofluorescent quantification of $MBP^+/O4^+$ cells at D55 showed a differentiation block of mutant cells (N=3-4, biological replicates). **J,** *PLP1* mutant cells showed an increased fraction of $Caspase\text{-}3^+/O4^+$ cells at D55 (N=3-4, biological replicates). **K-P**, Assessment of morphological complexity in $O4^+$ cells using Sholl analysis software. Immunofluorescent images of $O4^+$ cells were captured, then individual cell morphology was reconstructed by tracing the O4 stained branches assisted by Fiji plugin software Simple Neurite Tracer. Quantification showed failure of the mutant cells to achieve time-dependent increase in total traced length and ramification index (N=11-18 cells/treatment).

Figure 2. Gene correction in *PLP1^{G74E}* mutation rescues oligodendrocyte differentiation and axonal myelination. A, Schematic of co-culture system of human brain slice and EGFP-labeled, iPSC-derived OPCs. **B,** At 21 days after co-culture, iPSC-derived gene corrected oligodendrocytes ($EGFP^+/MBP^+$) showed similar morphologies as endogenous oligodendrocytes ($EGFP^-/MBP^+$). **C,** Classification of MBP^+ cells based on morphological complexity. **D,** *PLP1^{G74E}* mutant oligodendrocytes had mostly abnormal or immature morphologies (N=6-9 slices/ group, total number of transplanted oligodendrocytes pooled for analysis). **E,** For *in vivo* transplantation, $O4^+$ OPCs were purified by removal of $lectin^+$ nonspecific cells, followed by O4 immunopanning. Cells were transplanted into the cerebellum of postnatal immune-deficient *Shiverer* mice (N=3-4). **F,** MBP (green) and the human-specific antibody STEM121 (red) detected many corrected iPSC-derived oligodendrocytes after transplantation. **G-H,** Corrected cells engrafted and efficiently differentiated to MBP^+ oligodendrocytes whereas transplanted *PLP1^{G74E}* mutant cells failed to survive in the host brain. **I,** Electron microscopy of the transplanted area. Only thinly and loosely myelinated axons were found in *Shiverer* mouse transplanted with *PLP1^{G74E}* mutant cells. **J,** Electron microscopy of area transplanted with corrected cells revealed multi-layer, compact myelin.

Figure 3. Lack of evidence for ER stress, and evidence for abnormal iron metabolism and oxidative stress in in *PLP1^{G74E}* mutant OPCs. A, qPCR quantification of UPR and ER stress genes in *PLP1^{G74E}* mutant and corrected OPCs showed no significant difference with corrected cells (N=3-4, biological replicates). **B,D,** Little co-localization of mutant *PLP1^{G74E}* protein and the ER marker KDEL (arrows). **C,E,** Instead *PLP1^{G74E}* localized to fine processes (arrowheads) similar to wild type PLP1 in corrected cells (N=9 fields/group). **F,** Quantification of overlapping (colocalizing) staining with KDEL and PLP1 showed a trend but no significant difference between *PLP1^{G74E}* mutant and gene corrected oligodendrocytes. **G-L,** Evidence of *PLP1^{G74E}* protein transported out of ER to near O4+ cell surface locations. **M,** Induction of oxidative stress genes in *PLP1^{G74E}* mutant cells revealed by qPCR (N=4-5, biological replicates). **N-P,** Increased

levels of oxidative species in live OPCs detected with CellROX dye at D55 of differentiation (N=3, biological replicates).

Figure 4. Unique iron regulation and oxidative stress in human oligodendrocytes and *PLP1*^{G74E} mutation. A-C, Schematic of human oligodendrocyte isolation. Left: The brain tissue is dissociated into single cells, passed through lectin (BSL) and mouse IgM secondary antibody-coated plates to remove non-specific cells. O4$^+$ oligodendroccytes are then positively selected by attaching them to O4 coated plate. **D,** Isolated cells bound to O4 antibody showed other markers of oligodendrocyte markers such as OLIG2 and PDGFRα. **E**, qPCR quantification of iron regulatory genes in human endogenous O4$^+$ oligodendroccytes vs the rest of the neural cells unbound to the O4 antibody revealed an exceptionally high *TF* expression in oligodendrocytes. **F,** Quantification of oxidative stress gene expression in human O4$^+$ oligodendrocytes vs the rest of the neural cells by qPCR revealed naturally high level of oxidative stress in healthy human oligodendrocytes. **G,** Representative flow cytometry plot quantifying the level of TF receptor (TFRC) in O4$^+$ OPCs. **H**, Increased surface expression TFRC in mutant OPCs determined by flow cytometry (N=3-7, biological replicates). **I,** Abnormal expression of iron regulatory genes in mutant OPCs by qPCR (N=3-4, biological replicates). **J**, Western blot analysis of iron regulatory proteins (two pooled samples of N=3-4 biological replicates).

Figure 5. Iron chelation and lipophilic antioxidants rescue mutant cell survival and the differentiation block. A-D, In the baseline amount of TF or in the presence of iron-bound holo-TF, *PLP1*^{G74E} mutant O4$^+$ cells degenerated on D55. **E-F**, Reduction of free iron by apo-TF addition inhibited *PLP1*^{G74E} mutant O4$^+$ cell death but had no effect on corrected cells. **G-J**, Reduction of iron by the iron chelator deferoxamine (DFO) in presence of holo-TF also blocked cell death, similar to apo-TF. Additional iron administration counteracted the apo-TF effects. **K,** Quantification of O4$^+$ cells in all treatment groups by flow cytometry (N=3-4, biological replicates). **L-M**, Quantification of cell death and OPC differentiation in O4+ cells. **N-P,** Increased lipid ROS level in *PLP1*^{G74E} mutant cells was rescued by the presence of apo-TF or DFO to the levels of corrected cells (N=3-4, biological replicates). **Q-R**, Immunofluorescence quantification of MBP/O4$^+$ cells revealed that only the lipophilic antioxidants BHT or Trolox but not the hydrophilic antioxidants GSH or NAC, rescued the differentiation defect of *PLP1*^{G74E} mutant cells (N=3-4).

Figure 6. Iron chelation rescues phenotypes of *PLP1*^{G74E} mutation post transplantation and in slice explant culture. A, *PLP1*^{G74E} mutant and corrected OPCs were transiently (D35-55) treated with apo-TF or DFO before transplantation into the *Shiverer* mouse. **B-D**, Whereas untreated *PLP1*^{G74E} mutant OPCs failed to survive in the host brain, transient DFO and apo-TF treated OPCs survived and differentiated to mature MBP$^+$ oligodendrocytes (N=3). **E-G**, Ultrastructural assessment showed rescue of multi-layer myelination by the apo-TF and DFO-treated *PLP1*^{G74E} mutant OPCs. **H,** Schematic of treatment regimen of human slice co-cultures with DFO or apo-TF. **I-K,** Transient and long-term iron chelation rescued the differentiation block of *PLP1*^{G74E} mutant OPCs as seen by MBP staining of EGFP$^+$ cells (4-8 slices/treatment group, total number of transplanted oligodendrocytes pooled for analysis). **L,** Quantification of differentiation classes used the same criteria as in Fig. 2C-D.

Figure 7. Iron chelation rescues phenotypes of multiple *PLP1* mutations *in vitro* and *in vivo*. A, Treatment strategy to assess effects of DFO in additional human PMD mutations. **B-G,** Differentiation phenotype of additional human PMD mutations after treatment with DFO (N=3-4, biological replicates). B&E = T75P point mutation, C&F = Exon6 deletion, D&G = Duplication. **H,**

Jimpy mouse OPCs isolated at postnatal day 5-8 were tested for differentiation phenotype and transiently treated with iron chelation. **I-J,** *Jimpy* OPCs completely failed to differentiate upon removal of growth factors which was associated with increased cell death. **K-L,** Transient (4 day) DFO treatment rescued both differentiation and cell death as measured by Caspase-3 and MBP expression (N=10 fields/treatment from 2 biological replicates). **M,** *In vivo* iron chelation strategy in *Jimpy* mice. Subcutaneous injections with the brain-permeable iron chelator deferiprone (DFP) were given from postnatal day 7-14 and 21-death. **N-O,** Corpus callosum of vehicle-treated *Jimpy* mice at postnatal day 28 showed Caspase-3$^+$ apoptotic cells. **P-Q**, Electron microscopic analysis of corpus callosum in DFP- and vehicle-treated *Jimpy* mice showed surviving oligodendrocytes in the DFP-treated mice. Higher magnification of **P** and **Q** are depicted in **P'** and **Q'**, respectively. **R-W,** Fluorescent in situ hybridization (RNA scope) showed a significant reduction in *Atf4* and *Chop* gene expressions in Mbp+ mature oligodendrocytes after a 7-day *in vivo* DFP treatment from P7 in *Jimpy* mice (N = 3-4). **X-Y**, Immunostaining for Chop after a 7-day *in vivo* DFP treatment from P7 revealed a reduction in colocalization with pan-oligodendrocyte marker Olig2. **Z**, Western blot analysis of *Jimpy* brain showed significant reductions in UPR/ER stress markers Atf4 and phosphorylated Eif2α in DFP-treated *Jimpy* mice.

Supplementary Figure 1. Validation of pluripotency and normal karyotype in *PLP1^{G74E}* patient and corrected iPSCs. A, Subcutaneous injection of iPSCs in immunodeficient mice resulted in teratoma with three germ layers: ectoderm, endoderm, mesoderm. **B**, iPSCs express pluripotency markers OCT4 and TRA1-160 at the protein level. **C,** Both patient and corrected iPSCs show normal karyotype.

Supplementary Figure 2. Oligodendrocyte differentiation kinetics of *PLP1* mutants and corrected iPSCs. A, Schematic of oligodendrocyte differentiation protocol. **B**, An example of large variability among three original iPSC lines generated simultaneously from a patient with *PLP1^{T75P}* mutation, and their response to apo-TF and DFO. Clone 4 naturally made oligodendrocytes in response to standardized protocol, but clone 1 and 5 generated minimal number of oligodendrocytes. **C,** Two left data sets show six original iPSC clonal lines generated from a patient with *PLP1*^{G74E} mutation and their response to DFO treatment showing large variability, resulting in non-significant difference. Five datasets to the right show the phenotypic results of the clone 3 used in the gene correction to WT *PLP1* sequence that generated multiple subclones (3 shown here) that share the same culture history, which resulted in a much smaller variability. **D**, (Left) Validation of a single genomic integration of the targeting construct by Southern blot. Lane 1 shows a single band of an appropriate size. (Right) Detailed targeting construct design for *PLP1^{G74E}* mutation. The mutant endogenous sequence contained a single base pair mutation in exon3. The targeting construct with homologous arms shown in gray contained wildtype sequence for correction purpose. It also contained neomycin resistant gene flanked by loxP sites for drug screening purpose. The targeting construct was cloned into AAV vector. After drug selection, targeted locus was sequenced using PCR product, which was amplified with primer pairs shown in pink and green. These primer pairs distinguish endogenous vs targeted sequence by amplifying a fragment containing human genomic DNA and newly introduced neomycin resistant gene. Homologously targeted clones were then transiently transfected with Cre recombinase to remove neomycin cassette. **E,** Initial phase of oligodendrocyte differentiation in both *PLP1^{G74E}* mutant and corrected cells are similar, assessed by iPSC morphology (D0), SOX1$^{+/}$PAX6$^+$ neural rosette formation (D7), and NKX2.2$^+$/OLIG2$^+$ oligodendrocyte precursors (D11). **F**, Onset of PLP1 protein expression in O4+ cells occurs between day 35 and 45. **G,** Representative FACS plots for quantification of O4+ cells. **H,** Representative images of Caspase-3, colocalizing with O4$^+$ OPCs in *PLP1*^{G74E}.

Supplementary Figure 3. Lack of rescue in *PLP1*^{G74E} OPCs by UPR/ER stress inhibitors. **A**, ER stress inhibitors GSK2656157 or Kira6 was added to the culture and surviving O4$^+$ cells were quantified. The treatment did not rescue the mutant phenotype (N=3). **B**, Staining for ER stress marker CHOP in *Shiverer* mouse 12 weeks after transplantation of mutant cells shows no colocalization with transplanted oligodendrocytes (MBP$^+$).

Supplementary Figure 4. Iron chelation treatment rescues defective mutant OPC differentiation. A, Representative FACS plot for transferrin receptor in O4+ oligodendrocytes. **B-C**, In addition to DFO treatment shown in Fig. 5 G-H, an additional iron chelator deferiprone showed beneficial effects in the reduction of Caspase-3$^+$ OPC cell death and increase in MBP$^+$ differentiation in the mutant cells (N=3). **D-E**, Quantification of OPC cell death and differentiation in presence of treatment by apo-TF and DFO (N=3-4). **F**, Quantification of lipid ROS assay, in presence of chelation treatment by apo-TF and DFO (N=3-4). **G**, Out of the two lipophilic antioxidants BHT and Trolox that showed efficacy in rescuing mutant OPC differentiation, Trolox also reduced mutant cell death. A lipid oxidizing agent cumene hydroperoxide reversed the beneficial effect by apo-TF (N=3-5).

Supplementary Figure 5. *In vivo* Iron chelation rescues *Jimpy* oligodendrocytes. A-B, Representative images of WT and *Jimpy* primary OPCs treated with vehicle or DFO. **C,** Kaplan-Meyer survival curve of DFP-treated *Jimpy* mice shows a significant increase of lifespan by DFP treatment ($p = 0.047$, N=7 treated group, N=11 untreated group). **D,** Complete blood counts (CBC) for determination of DFP dose. All parameters in CBC showed a dose-dependent anemic effect. A clinically relevant 30mg/kg was chosen with one week break for DFP *in vivo* experiment. **E,** Brains of *Jimpy* mice treated with vehicle or 30mg/kg/day DFP were collected at postnatal day 28 and cerebellar white matter was analyzed for reactive astrocytes (GFAP) and microglia (Iba1) activation. **F,** Quantification showed a significant reduction in inflammatory response in DFP-treated mice (N=3). **G-J,** Fluorescent in situ hybridization (RNA scope) showed a significant reduction in *Atf4* and *Chop* gene expressions in PDGFRα+ OPC after a 7-day *in vivo* DFP treatment from P7 in *Jimpy* mice (N = 3-4).

References

Back, S.A., Gan, X., Li, Y., Rosenberg, P.A., and Volpe, J.J. (1998). Maturation-dependent vulnerability of oligodendrocytes to oxidative stress-induced death caused by glutathione depletion. The Journal of neuroscience : the official journal of the Society for Neuroscience *18*, 6241-6253.
Brissot, P., and Loreal, O. (2016). Iron metabolism and related genetic diseases: A cleared land, keeping mysteries. Journal of hepatology *64*, 505-515.
Butts, B.D., Houde, C., and Mehmet, H. (2008). Maturation-dependent sensitivity of oligodendrocyte lineage cells to apoptosis: implications for normal development and disease. Cell death and differentiation *15*, 1178-1186.
Dautigny, A., Mattei, M.G., Morello, D., Alliel, P.M., Pham-Dinh, D., Amar, L., Arnaud, D., Simon, D., Mattei, J.F., Guenet, J.L., *et al*. (1986). The structural gene coding for myelin-associated proteolipid protein is mutated in jimpy mice. Nature *321*, 867-869.
Dhaunchak, A.S., and Nave, K.A. (2007). A common mechanism of PLP/DM20 misfolding causes cysteine-mediated endoplasmic reticulum retention in oligodendrocytes and Pelizaeus-Merzbacher disease. Proceedings of the National Academy of Sciences of the United States of America *104*, 17813-17818.
Diecke, S., Lu, J., Lee, J., Termglinchan, V., Kooreman, N.G., Burridge, P.W., Ebert, A.D., Churko, J.M., Sharma, A., Kay, M.A., *et al*. (2015). Novel codon-optimized mini-intronic plasmid for efficient, inexpensive, and xeno-free induction of pluripotency. Scientific reports *5*, 8081.
Dixon, S.J., Lemberg, K.M., Lamprecht, M.R., Skouta, R., Zaitsev, E.M., Gleason, C.E., Patel, D.N., Bauer, A.J., Cantley, A.M., Yang, W.S., *et al*. (2012). Ferroptosis: an iron-dependent form of nonapoptotic cell death. Cell *149*, 1060-1072.
Douvaras, P., and Fossati, V. (2015). Generation and isolation of oligodendrocyte progenitor cells from human pluripotent stem cells. Nature protocols *10*, 1143-1154.
Elitt, M.S., Shick, H.E., Madhavan, M., Allan, K.C., Clayton, B.L.L., Weng, C., Miller, T.E., Factor, D.C., Barbar, L., Nawash, B.S., *et al*. (2018). Chemical Screening Identifies Enhancers of Mutant Oligodendrocyte Survival and Unmasks a Distinct Pathological Phase in Pelizaeus-Merzbacher Disease. Stem cell reports *11*, 711-726.
Espinosa de los Monteros, A., Kumar, S., Zhao, P., Huang, C.J., Nazarian, R., Pan, T., Scully, S., Chang, R., and de Vellis, J. (1999). Transferrin is an essential factor for myelination. Neurochemical research *24*, 235-248.
Feng, H., and Stockwell, B.R. (2018). Unsolved mysteries: How does lipid peroxidation cause ferroptosis? PLoS Biol *16*, e2006203.
Gupta, N., Henry, R.G., Strober, J., Kang, S.M., Lim, D.A., Bucci, M., Caverzasi, E., Gaetano, L., Mandelli, M.L., Ryan, T., *et al*. (2012). Neural stem cell engraftment and myelination in the human brain. Science translational medicine *4*, 155ra137.
Hansen, D.V., Lui, J.H., Parker, P.R., and Kriegstein, A.R. (2010). Neurogenic radial glia in the outer subventricular zone of human neocortex. Nature *464*, 554-561.
Harrington, E.P., Zhao, C., Fancy, S.P., Kaing, S., Franklin, R.J., and Rowitch, D.H. (2010). Oligodendrocyte PTEN is required for myelin and axonal integrity, not remyelination. Annals of neurology *68*, 703-716.
Hayflick, S.J., Hartman, M., Coryell, J., Gitschier, J., and Rowley, H. (2006). Brain MRI in neurodegeneration with brain iron accumulation with and without PANK2 mutations. AJNR Am J Neuroradiol *27*, 1230-1233.

Hentze, M.W., Muckenthaler, M.U., Galy, B., and Camaschella, C. (2010). Two to tango: regulation of Mammalian iron metabolism. Cell *142*, 24-38.
Hobson, G.M., and J., K. (1999). PLP1-Related Disorders.
Ikeda, M., Hossain, M.I., Zhou, L., Horie, M., Ikenaka, K., Horii, A., and Takebayashi, H. (2016). Histological detection of dynamic glial responses in the dysmyelinating Tabby-jimpy mutant brain. Anat Sci Int.
Khorchid, A., Fragoso, G., Shore, G., and Almazan, G. (2002). Catecholamine-induced oligodendrocyte cell death in culture is developmentally regulated and involves free radical generation and differential activation of caspase-3. Glia *40*, 283-299.
Kramer-Albers, E.M., Gehrig-Burger, K., Thiele, C., Trotter, J., and Nave, K.A. (2006). Perturbed interactions of mutant proteolipid protein/DM20 with cholesterol and lipid rafts in oligodendroglia: implications for dysmyelination in spastic paraplegia. The Journal of neuroscience : the official journal of the Society for Neuroscience *26*, 11743-11752.
Kruer, M.C., Paisan-Ruiz, C., Boddaert, N., Yoon, M.Y., Hama, H., Gregory, A., Malandrini, A., Woltjer, R.L., Munnich, A., Gobin, S., *et al*. (2010). Defective FA2H leads to a novel form of neurodegeneration with brain iron accumulation (NBIA). Annals of neurology *68*, 611-618.
Leitner, D.F., and Connor, J.R. (2012). Functional roles of transferrin in the brain. Biochimica et biophysica acta *1820*, 393-402.
Maly, D.J., and Papa, F.R. (2014). Druggable sensors of the unfolded protein response. Nat Chem Biol *10*, 892-901.
Naguib, Y.M. (1998). A fluorometric method for measurement of peroxyl radical scavenging activities of lipophilic antioxidants. Anal Biochem *265*, 290-298.
Nevin, Z.S., Factor, D.C., Karl, R.T., Douvaras, P., Laukka, J., Windrem, M.S., Goldman, S.A., Fossati, V., Hobson, G.M., and Tesar, P.J. (2017). Modeling the Mutational and Phenotypic Landscapes of Pelizaeus-Merzbacher Disease with Human iPSC-Derived Oligodendrocytes. American journal of human genetics *100*, 617-634.
Numasawa-Kuroiwa, Y., Okada, Y., Shibata, S., Kishi, N., Akamatsu, W., Shoji, M., Nakanishi, A., Oyama, M., Osaka, H., Inoue, K., *et al*. (2014). Involvement of ER stress in dysmyelination of Pelizaeus-Merzbacher Disease with PLP1 missense mutations shown by iPSC-derived oligodendrocytes. Stem cell reports *2*, 648-661.
Recalcati, S., Alberghini, A., Campanella, A., Gianelli, U., De Camilli, E., Conte, D., and Cairo, G. (2006). Iron regulatory proteins 1 and 2 in human monocytes, macrophages and duodenum: expression and regulation in hereditary hemochromatosis and iron deficiency. Haematologica *91*, 303-310.
Roach, A., Boylan, K., Horvath, S., Prusiner, S.B., and Hood, L.E. (1983). Characterization of cloned cDNA representing rat myelin basic protein: absence of expression in brain of shiverer mutant mice. Cell *34*, 799-806.
Siah, C.W., Trinder, D., and Olynyk, J.K. (2005). Iron overload. Clin Chim Acta *358*, 24-36.
Sidman, R.L., Dickie, M.M., and Appel, S.H. (1964). Mutant Mice (Quaking and Jimpy) with Deficient Myelination in the Central Nervous System. Science *144*, 309-311.
Sistermans, E.A., de Wijs, I.J., de Coo, R.F., Smit, L.M., Menko, F.H., and van Oost, B.A. (1996). A (G-to-A) mutation in the initiation codon of the proteolipid protein gene causing a relatively mild form of Pelizaeus-Merzbacher disease in a Dutch family. Human genetics *97*, 337-339.
Southwood, C.M., Garbern, J., Jiang, W., and Gow, A. (2002). The unfolded protein response modulates disease severity in Pelizaeus-Merzbacher disease. Neuron *36*, 585-596.

Stephenson, E., Nathoo, N., Mahjoub, Y., Dunn, J.F., and Yong, V.W. (2014). Iron in multiple sclerosis: roles in neurodegeneration and repair. Nature reviews Neurology *10*, 459-468.
Woodward, K.J. (2008). The molecular and cellular defects underlying Pelizaeus-Merzbacher disease. Expert reviews in molecular medicine *10*, e14.
Zhang, Y., Chen, K., Sloan, S.A., Bennett, M.L., Scholze, A.R., O'Keeffe, S., Phatnani, H.P., Guarnieri, P., Caneda, C., Ruderisch, N., *et al*. (2014). An RNA-sequencing transcriptome and splicing database of glia, neurons, and vascular cells of the cerebral cortex. The Journal of neuroscience : the official journal of the Society for Neuroscience *34*, 11929-11947.

Methods

iPSC generation and culture

Fibroblasts from two PMD patients enrolled in a clinical study (Clinicaltrials.gov identifier NCT01005004) were obtained under approval from UCSF Institutional Review Board (IRB) (Study Protocol13-10806). All iPSC lines were established by electroporation of a CoMiP episomal vector containing 4 reprogramming factors (OCT4, KLF4, SOX2, and c-MYC) following a published protocol[1].

iPSCs were maintained on CF1 MEF feeder cells in ES medium containing Knockout DMEM/F12, 20% knockout serum replacement, non-essential amino acids, Glutamax (Life Technologies), and 10ng/ml human basic FGF (peprotech). Pluripotency was confirmed by expression of TRA1-60 (Cell Signaling), OCT3/4 (Santa Cruz Biotechnology), as well as teratoma formation and differentiation into ectoderm, mesoderm, and endoderm lineages. A normal karyotype was confirmed in all lines. Mycoplasma contamination has been confirmed negative in all iPSC lines.

Gene targeting

*AAV plasmid and targeting vector design***.** 5' homologous arm (1.2kb) containing wildtype *PLP1* exon 3 sequence, and 3' homologous arm (1.3K) containing intron 3 sequence were amplified from genomic DNA of the patient's father by PCR. A PGK promoter and neomycin resistance cassette flanked by two loxP sites was inserted between 5' and 3' homologous arms. Please see Extended Data Figure 14 for annotated complete sequence of the targeting vector. The construct was cloned into pAAV packaging plasmid.

*AAV viral preparation***.** AAV was produced using a highly recombinogenic AAV-DJ AAV serotype[2] in HEK293T cells as described[3]. pAAV containing wildtype *PLP1* sequence, pHelper, and pRC-DJ were co-transfected and three days later, HEK293T cells were collected, suspended in benzonase buffer, and subjected to 3 rounds of freeze-thaw cycles to homogenize the cells. Homogenate was incubated with benzonase to digest DNA, spun at 5000RCF for 15min, and the supernatent containing AAV was used for iPSC infection.

AAV transduction of iPSCs. iPSCs were infected by seeding 0.25×10^6 cells plated on to matrigel coated 6-well plate in NutriStem XF/FF Culture medium (Stemgent). One day after infection, medium was changed to ES cell medium and MEF feeder cells were added. Two to three days after infection, neomycin (100ug/ml) was added to the culture for approximately 1 week.

*Validation of targeting***.** Neomycin resistant iPSC colonies presumably incorporated the targeting vector were manually picked, expanded, and checked for homologous recombination by PCR using primers designed to detect recombination junctions spanning endogenous *PLP1* allele and non-endogenous neomycin resistance gene, or PGK promoter. The primer locations are depicted in pink and green arrows in Extended Data Figure 3b. Following this initial PCR screen, the mutant locus was sequenced to confirm the gene correction to wildtype sequence. To exclude the possibility of multiple integrations, Southern blot analysis using a probe against neomycin resistance gene was performed. The 300bp probe template was obtained from digestion of the targeting pAAV plasmid with PSTI and SapI followed by gel extraction. The P32 labeled probe was made with Klenow labelin kit (Agilent) and purified with microspin columns (GE Healthcare Life Sciences). 10ug of genomic DNA was digested overnight with EcoRI and separated by electrophoresis. DNA was blotted on to a nylon membrane and crosslinked. The neomycin probe was incubated for 3 hours at 65ºC. Following washes, signals were detected by autoradiography film (Kodak). After confirmation of a single integration of the targeting construct, the neomycin resistant gene was excised by transfecting a Cre expression plasmid

containing puromycin resistant gene with FuGENE6 (Promega). Three days post transfection, puromycin (1ug/ml) was added to the medium for 2 days to select Cre expressing colonies. Resistant colonies were picked and evaluated for neomycin sensitivity and loss of neomycin sequences by genomic PCR. Complete *PLP1* cDNA was sequenced to confirm intact splice sites.

OPC differentiation

A previously published protocol for directed iPSC differentiation to OPCs[4] was used with the following modifications: human ES cell medium and human ES cell medium without basic FGF were used in place of mTeSR and custom mTeSR, respecitvely. The concentration of SAG was 0.5uM, T3 was 40ng/ml, NT3 was 1ng/ml. Penicillin-Streptomycin was omitted from N2 medium, HGF from PDGF medium, and HEPES from Glia medium. When apo-TF or holo-TF was used in PDGF medium and Glia medium, commercially available N2 supplement (Life Technologies) was replaced with: 6.3ng/ml progesterone, 5.2ng/ml selenite, 16.11ug/ml putrescene, 5ug/ml human insulin, and 150ug/ml human TF (either apo- or holo- form, R&D).

On day 0, iPSCs between passage 18 and 20 were plated at $0.25X10^6$/well on a matrigel-coated 6-well plate with ES medium without basic FGF, supplemented with dual SMAD inhibitors, RA, and ROCK inhibitor thiazovivin (Santa Cruz). From day 1 to day 4, N2 medium was gradually increased by 25% each day, reaching 100% on day 4. On day 8, dual SMAD inhibitors were replaced with SAG. On day 12, cells were lifted, dissociated, and seeded on petri dishes for sphere formation. On day 20, the medium was changed to PDGF medium. On day 30, spheres were plated on poly-L-ornithine/laminin-coated plates. On day 45, the medium was changed to Glia medium. Most differentiation assays were conducted at day 55 unless otherwise stated.

Small molecules and peptide treatments

The following drugs were added to OPC differentiation culture from day 35 to 55: apo-TF (R&D 3188-AT, 150ug/ml), holo-TF (R&D 2914-HT, 150ug/ml), deferoxamine (Sigma D9533, 10uM), deferiprone (Sigma 379409, 30uM), GSH (Sigma G4251, 1mM), NAC (Sigma A9165, 0.25mM), BHT (Sigma 47168, 100uM), Trolox (Sigma 238813, 60uM), cumene hydroperoxide (Component of Life Technologies C10446, 1:5000), Ferrostatin-1 (Tocris 5180, 300nM), Liproxstatin-1 (Sigma SML141, 300nM), RSL-3 (Cayman chemical 19288, 10nM), Ammonium iron citrate (Sigma F5879, 5ug/ml), Ferric citrate (Sigma F3388, 15uM), Manganase chloride (Sigma M8054, 15uM), Cobalt chloride (Sigma 255599, 15uM), Nickel Sulfate (Sigma 227676, 15uM), GSK2656157 (EMD Millipore 5046510001, 200nM), Kira6 (from Papa lab, UCSF, 50nM).

***In vivo* Cell transplantation**

All data shown involving animal procedures were performed according to protocols approved by the Stanford University Institutional Animal Care and Use Committee. Initially, we transplanted unpurified neural progenitor cells at around days 60-80 of the differentiation protocol into *Shiverer* mice. However, the overproliferation presumably of more primitive cells complicated the analysis. We therefore purified O4+ cells at day 55 from the bulk culture by immunopanning (see method described below). 12,000 O4-immunopanned cells/site in 0.5ul volume were transplanted in postnatal day 1 of *Shiverer;Rag2*$^{-/-}$ mice. Site of transplantation was cerebellar white matter, identified by coordinates (0.9mm medial-lateral, 3.0mm posterior,1.8mm ventral) from lambda. Animals were sacrificed by transcardiac perfusion with 4% PFA + 0.25% glutaraldehyde at 13 week post transplantation, and 50um sagittal brain sections were used for immunohistochemistry. Quantification of stained MBP and human specific marker STEM121 was done by calculating % STEM121+ cells that coloalize with MBP staining.

OPC differentiation on human slice culture
Fetal cortical tissue (gestational weeks 20 to 23) was collected from elective pregnancy termination specimens at San Francisco General Hospital with previous patient consent. Research protocols were approved by the Committee on Human Research (Institutional Review Board) at University of California, San Francisco. Human slice culture was prepared as described[5]. Cultured iPSC-derived spheres at day 40-45 were dissociated with accutase, resuspended in PDGF medium, and labeled with GFP lenti virus overnight. Cells were washed twice to remove viral particles, resuspended in approximately 6ul DMEM/F12, and plated onto human slice culture prepared a day before. Three weeks post plating, a subset of the grafted cells gave rise to $NeuN^+$ neurons, with a similar efficiency between mutant and corrected cells (Extended Data Fig. 6b). Another fraction of the $EGFP^+$ cells differentiated to MBP expressing mature oligodendrocytes. Slice culture was fixed with 4% PFA for 15min, cryoprotected, and sectioned at 14um for immunohistochemistry. To quantitatively assess the degree of oligodendrocyte maturation, we classified the $EGFP^+/MBP^+$ cells into three categories based on morphological complexity (differentiated, immature, abnormal).

***Jimpy in vitro* OPC differentiation assay**
Cortical OPCs were immunopurified from postnatal day 5-8 *Jimpy* or wildtype littermate mice as described[6]. After 3 days in culture with proliferation factor PDGF-AA, OPCs were directed to differentiate by removal of PDGF-AA and addition of a differentiation factor T3. Cells were fixed 24hrs after initiation of differentiation for histological analysis. Deferoxamine was added to media throughout the four-day culture at 10uM concentration.

***Jimpy in vivo* iron chelation treatment**
Jimpy mice were subcutaneously injected with 30mg/kg deferiprone (Sigma 379409) in sterile PBS, during P7 to P14 and P21 to P28 for survival study, and P7 to P14 for ER stress/UPR study. Care was taken to minimize disturbance of the mice during injection to avoid seizures. For histological assays requiring electron microscopy assay, brains were collected after cardiac perfusion with 4% PFA containing 0.25% glutaldehyde at P28 and sectioned with a vibratome. Quantification of GFAP and Iba1 was done by calculating fluorescent intensity in stained sections.

Fluorescent in situ hybridization
Three-color smFISH was performed on corpus collosum containing fixed frozen sections from *Jimpy* mice using Advanced Cell Diagnostics RNAscope® Fluorescent Multiplex Reagent Kit and probes. Briefly, cryosections (14µm thick) were mounted on glass slides and washed in RNase free PBS for 5 mins and baked at 60°C for 30 mins and were further fixed in 4% neutral buffered paraformaldehyde for 15 min at 4°C. Next, sections were dehydrated in 50%, 70% and 100% ethanol for 5 mins at room temperature and air dried. Target retrieval was then performed with RNAscope reagents for 3 mins at 95 °C and sections were further washed with distilled water followed by washes in 100% ethanol 2-3 times. After drying, sections were permeabilized with Protease IV reagent for 15 mins at 40°C, washed and maintained in RNase free water until hybridization step. Probes (Mm-Atf4 (405101), Mm-Pdgfra-C2 (480661-C2), Mm-Ddit3-C3 (317661-C3); C2 and C3 probes were diluted at 1:50 ratio in channel 1 probe) were mixed and preheated to 40°C for 5 mins and then added to the sections for 2hr at 40°C. After probe hybridization, sections were washed two times 2 mins each and further incubated in AMP 1-FL for 30 min at 40°C, washed two times, incubated in RNAscope AMP 2-FL for 15 min at 40°C, washed two times, incubated in RNAscope AMP 3-FL for 30 min at 40°C, washed two times and incubated in AMP 4-FL-Alt B solution for 15 mins at 40°C, washed two times and counterstained with RNAscope DAPI for 30 seconds. All wash steps were performed with RNAscope 1x wash buffer. Where indicated, after the RNAscope

assay, the slides were blocked in 5% Horse serum/0.05% TX-100 in PBS, followed by 1 hr of primary antibody incubation at RT, followed by three washes in PBS and secondary antibody incubation for 1hr at RT and mounted with prolong gold antifade. Quantification of RNA spots was performed on images acquired at 63x on Lecia SP5 upright AOBS confocal microscope.

Antibodies

Following primary antibodies were used.
Olig2 (courtesy of Charles Stiles)
NKX2.2(Developmental Studies Hybridoma Bank 74.5A5)
SOX1 (R&D AF3369)
PAX6 (Developmental Studies Hybridoma Bank Pax6)
O4 (Mouse hybridoma)
PLP1 (Abcam)
MBP (AbD Serotec MCA409S)
Cleaved Caspase-3 (Cell Signaling 9664S)
KDEL (Abcam ab50601)
GFP (Aveslab GFP-1020)
Human cytoplasmic (Clontech STEM121)
NeuN (EMD Millipore MAB377)
PDGFRa (BD Bioscience 556001)
Transferrin (Abcam ab137744)
Ferritin (Novus Biologicals NB600-920)
IRP1 (Cell Signaling 20272)
IRP2 (Cell Signaling 37135S)
Transferrin receptor (BD Bioscience 561939)
Ferroportin (Novus Biologicals NBP1-21502)
beta Actin (Sigma A5441)
GFAP (Fisher 13-0300)
Iba1 (Wako 019-19741)
Eif2α (Cell Signaling 9722)
Phospho-Eif2α (Fisher MA5-15133)
ATF4 (Aviva Systems Biology ARP37017)
CHOP (Fisher MA1-250)

Secondary antibodies of appropriate species were purchased from Jaxon ImmunoResearch and Life Technologies.

qPCR primers

For quantitative PCR, total RNA was isolated at described time points with Trizol reagent (Life Technologies) or RNAeasy Mini Kit (Qiagen) following manufacturer's protocols. Contaminating DNA was removed with TURBO DNA-free kit (Life Technologies). cDNA was obtained with High-capacity cDNA reverse transcription kit (Life Technologies). SYBR green-based qPCR was conducted in LightCycler 480 with manufacturer's reagents (Roche) with the following primer sets:

PAX6 FW: TTTGCCCGAGAAAGACTAGC RV: CATTTGGCCCTTCGATTAGA
OLIG2 FW: TGCGCAAGCTTTCCAAGAT RV: CAGCGAGTTGGTGAGCATGA
SOX1 FW: GGAATGGGAGGACAGGATTT RV: AACAGCCGGAG CAGAAGATA
NKX2.2 FW: GACAACTGGTGGCAGATTTCGCTT RV: AGCCACAAAGAAAGGAGTTGGACC
Spliced XBP1 FW: CTGAGTCCGCAGCAGGTGCAG RV: GGTCCAAGTTGTCCAGAATGCCC
BIP FW: CCGCTGAGGCTTATTTGGGA RV: TCTTTGGTTGCTTGGCGTTG

ATF3 FW: CTCGGGGTGTCCATCACAAA RV: TTGTTTCGGCACTTTGCAGC
HMOX1 FW: GAGGAACTTTCAGAAGGGCCA RV: CCTTGTTGCGCTCAATCTCC
SOD3 RW: GTGCAGCTCTCTTTTCAGGAG RV: GAGCAGGCAGGAACACAGTAG
ATOX1 FW: CGGGTCCTCAATAAGCTTGGA RV: AGGGTTGCAAGCAGAGTGTC
SCARA3 FW: CCGAAGACATCTCCTTGACCC RV: GCAGTTGTTCAGGGCTTTCG
TXNIP RW: ACCTGCGCTATGAAGACACG RV: AAGCTCAAAGCCGAACTTGT
SOD2 FW: GTTGGGGTTGGCTTGGTTTC RV: CCCCAGCAGTGGAATAAGGC
TXN FW: GGACGCTGCAGGTGATAAAC RV: CGTTGGAATACTTTTCAGAGAGGG
TXNRD2 FW: ATGATCTCCTGGTGGTCGGC RV: TGGGGAGAAGGTTCCACGTA
TF FW: GATGCTTACCTGGCTCCCAATAAC RV: CTTCTTCACCACAGCAACAGCAT
IRP1 FW: CTTGGGTCAGGTTCGCCG RV: TCCAGGATGGTGGAAACTGC
IRP2 FW: GGCAGAAATCGAGAGAGGCT RV: TGAGCCATTCCAGTTCCAGG
TFRC FW: TTGGACATGCTCATCTGGGG RV: CCTGATGACCGAGATGGTGG
APP FW: GATCCCAAGAAAGCCGCTCA RV: CACTGCAGGCACGTTGTAGA
CP FW: AGCTGGAACAGAGGATTCTGC RV: GACAAACAATCAGGGGGCCA
P53 FW: ACCTATGGAAACTACTTCCTGAAAA RV: CAATATCGTCCGGGGACAGC
SAT1 FW: CAGTGACATACTGCGGCTGAT RV: AGGGGTGCTCTCCAAAACC
PLP1 FW: TATCTCATCAATGTGATCCATGCCT RV: TCCTAGCCATTTTCCCAAACAAT
DM20 FW: TATCTCATCAATGTGATCCATGCCT RV: CCACAAACGTTGCGCTCA

Electron Microscopy
Animals were cardiacly perfused with 4% PFA containing 0.25% glutaldehyde. Alternative vibratome sections were kept for immunohistochemistry and EM, which were post-fixed in 4% glutaraldehyde for several days. Regions of interest determined by immunohistochemistry were micro-dissected, fixed in 2% osmium tetroxide and embedded in resin. Ultrathin sections were placed onto copper grids, stained with uranyl acetate and lead, and examined with a Hitachi H-600 or TEM 1400 Transmission Electron Microscopes. Use of TEM 1400 was supported by NIH grant SIG number 1S10RR02678001.

Flow Cytometry
The bulk culture was detached using Accutase, dissociated, rinsed, and resuspended in PBS containing1% BSA. Cells were incubated with O4-APC (Miltenyi Biotec Inc 130-099-211) and TFRC-GFP (BD Biosciences 561939) for 10min at room temperature. Following a wash with PBS, cells were suspended in PBS containing 5mM EDTA and analyzed with FACSAria II Cell Sorter (BD Biosciences) and FACSDiva software (BD Biosciences). Dead cells were excluded by Dapi staining.

Morphological complexity assessment
Cultures at described days were live-stained with O4 antibody for 30min, followed by Cy3-conjugated secondary antibody for 30min. After fixation, images were taken at 40X magnification in Leica microscope equipped with CCD camera. Individual cell morphology was reconstructed by tracing the O4 stained branches assisted by a Fiji plugin software Simple Neurite Tracer[7]. Traced images were analyzed with Sholl analysis software (Fiji)[8]. Ramification index, which integrates the number of branches from soma and number of intersections, as well as the total length of traced line were presented in results.

Reactive oxygen species assessment

General ROS assessment: After live O4 staining to identify OPCs, the CellROX® ROS sensor (Life Technologies) was used at 1:500 dilution of the ROX reagent following manufacturer's protocol, with a following modification: incubation with ROX reagent was increased to 60min. Lipid ROS assessment: Click-iT® Lipid Peroxidation Detection with Linoleamide Alkyne (LAA) (Life Technologies) was used following manufacturer's protocol with the following modifications: LAA stock solution was added to the culture at 10uM concentration from day 49 to 55 every other day. On day 55, cultures were live-stained with O4 first, then manufacturer's LAA detection protocol was followed. Quantification of LAA+ cells was conducted under Leica microscope equipped with CCD camera within 2 days of detection.

Western blot analysis
Isolated 50,000 O4+ oligodendrocytes were pelleted and snap frozen until analysis. Cell pellet was homogenized in lysis buffer, separated by electrophoresis following manufacturer's protocol (Bolt Mini gel, Thermo Fisher), transferred, and incubated with primary antibodies overnight. Proteins were visualized using Licor Western blot detection system.

Isolation of human primary OPCs
Fetal brain tissues described in the human slice culture section was dissociated with papain for 10min. Single cell suspension was passed onto series of culture dishes coated with BSL (Bandeiraea Simplicifolia Lectin I, Vector Laboratories L1100) to remove microglia and endothelial cells, IgM secondary antibody (Jackson immunolab 115-005-020) to avoid non-specific binding, and O4 (Mouse hybridoma), to isolate $O4^+$ OPCs. At the end of O4 binding, adherent cells were washed, and detached with Trypsin, and collected by centrifugation. Cells were directly homogenized in Trizol for RNA collection.

Statistics
Each *in vitro* experiment was repeated at least three times. 2-to-3 biological replicates were included in each experiment.
In vivo experiments were repeated using at least randomly assigned 5 mice per treatment group, considering unexpected dropout often due to strain vulnerability to seizures. For statistical analysis, two sided one way ANOVA and t-test with normal distribution, log-rank survival test, or one way Chi-square tests were used as appropriate. * indicates p-value<0.05, ** p-value<0.01, *** p-value<0.001, n.s. = not significant. Data are presented as mean ± SEM.

Data Availability
The data that support the findings of this study are available from the corresponding author upon reasonable request.

References:

1 Diecke, S. *et al*. Novel codon-optimized mini-intronic plasmid for efficient, inexpensive, and xeno-free induction of pluripotency. *Scientific reports* **5**, 8081, doi:10.1038/srep08081 (2015).
2 Melo, S. P. *et al*. Somatic correction of junctional epidermolysis bullosa by a highly recombinogenic AAV variant. *Molecular therapy : the journal of the American Society of Gene Therapy* **22**, 725-733, doi:10.1038/mt.2013.290 (2014).

3 Xu, W. *et al*. Distinct neuronal coding schemes in memory revealed by selective erasure of fast synchronous synaptic transmission. *Neuron* **73**, 990-1001, doi:10.1016/j.neuron.2011.12.036 (2012).
4 Douvaras, P. & Fossati, V. Generation and isolation of oligodendrocyte progenitor cells from human pluripotent stem cells. *Nature protocols* **10**, 1143-1154, doi:10.1038/nprot.2015.075 (2015).
5 Hansen, D. V., Lui, J. H., Parker, P. R. & Kriegstein, A. R. Neurogenic radial glia in the outer subventricular zone of human neocortex. *Nature* **464**, 554-561, doi:10.1038/nature08845 (2010).
6 Harrington, E. P. *et al*. Oligodendrocyte PTEN is required for myelin and axonal integrity, not remyelination. *Annals of neurology* **68**, 703-716, doi:10.1002/ana.22090 (2010).
7 Frangi, F., Niessen, W.J., Vinc, K.L., Viergever, M.A. Multiscale vessel enhancement filtering. In Medical Image Computing and Computer-Assisted Intervention *Computer Science* **1946**, 130-137 (1998).
8 Ferreira, T. A. *et al*. Neuronal morphometry directly from bitmap images. *Nature methods* **11**, 982-984, doi:10.1038/nmeth.3125 (2014).

Figure 1

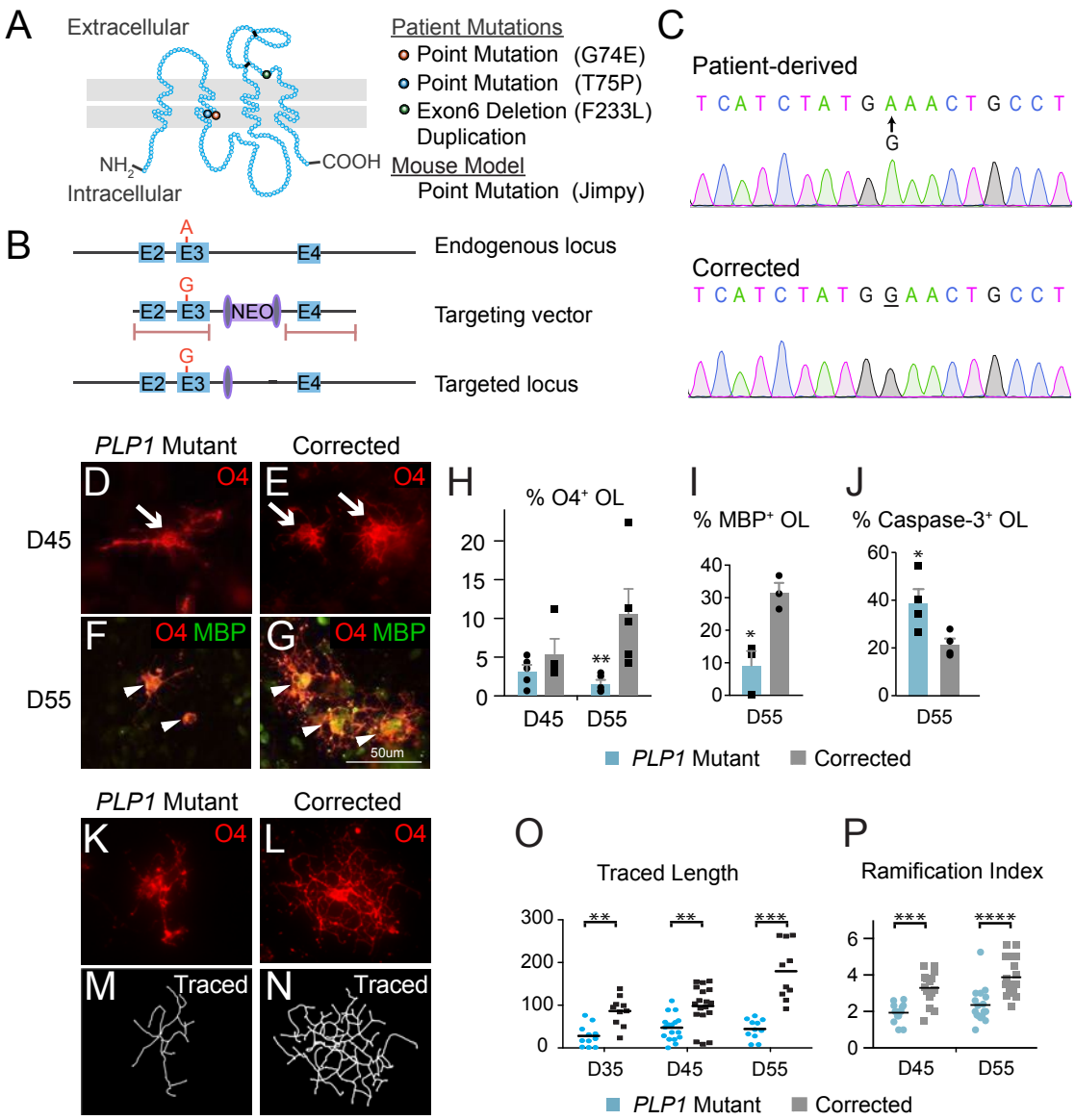
A
Extracellular
Intracellular
NH2
COOH
Patient Mutations
Point Mutation (G74E)
Point Mutation (T75P)
Exon6 Deletion (F233L)
Duplication
Mouse Model
Point Mutation (Jimpy)
B
E2 E3 E4
Endogenous locus
E2 E3 NEO E4
Targeting vector
Targeted locus
C
Patient-derived
T C A T C T A T G A A A C T G C C T
G
Corrected
T C A T C T A T G G A A C T G C C T
PLP1 Mutant
Corrected
D45
D55
O4
O4 MBP
50um
H
% O4+ OL
I
% MBP+ OL
J
% Caspase-3+ OL
PLP1 Mutant
Corrected
K
L
M
Traced
N
Traced
O
Traced Length
D35
D45
D55
P
Ramification Index

Figure 2

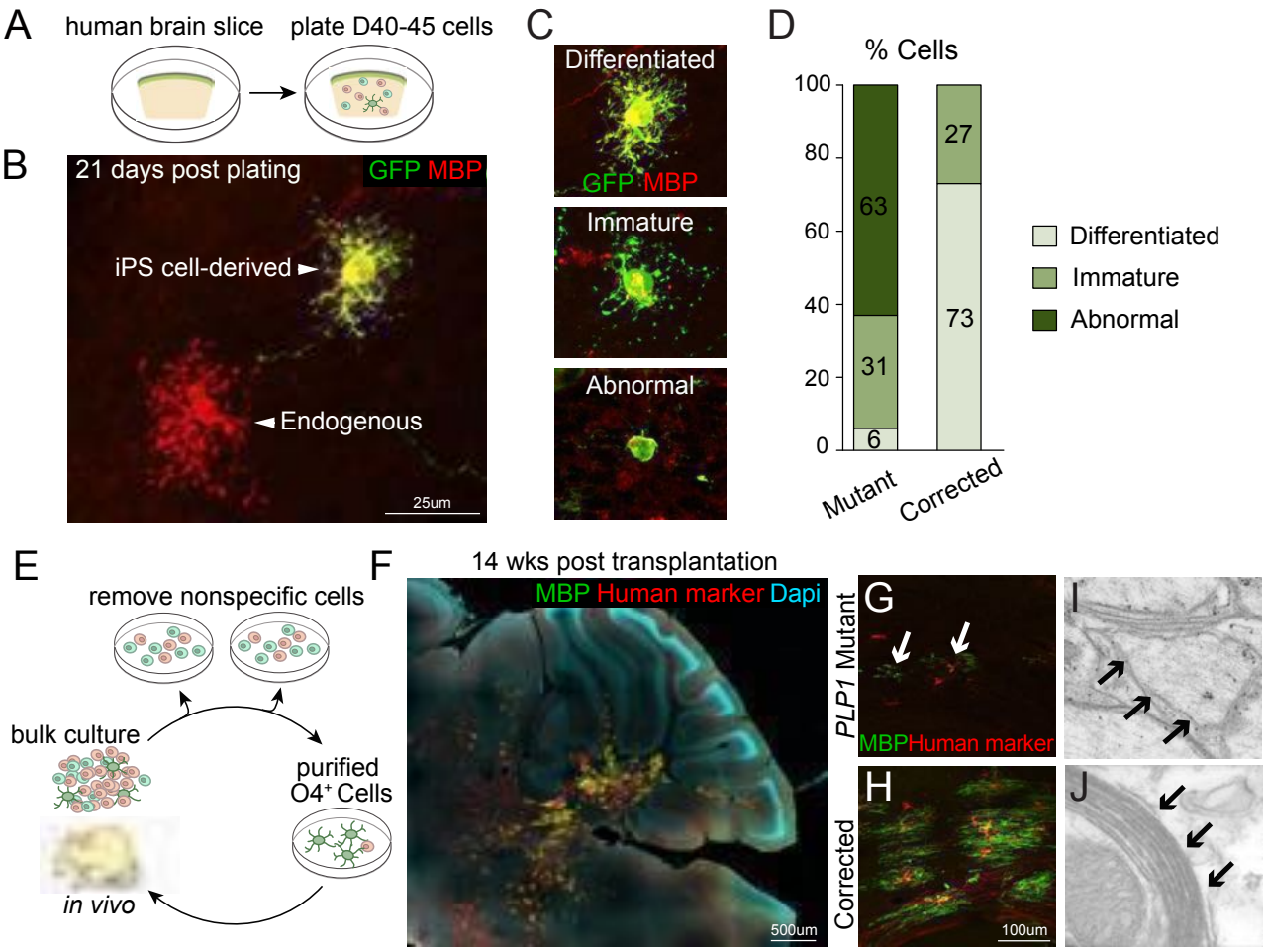
A
human brain slice
plate D40-45 cells
B
21 days post plating
GFP MBP
iPS cell-derived
Endogenous
25um
C
Differentiated
GFP MBP
Immature
Abnormal
D
% Cells
100
80
60
40
20
0
63
31
6
27
73
Mutant
Corrected
Differentiated
Immature
Abnormal
E
remove nonspecific cells
bulk culture
purified
O4+ Cells
in vivo
F
14 wks post transplantation
MBP Human marker Dapi
500um
PLP1 Mutant
G
MBPHuman marker
Corrected
H
100um
I
J

Figure 3

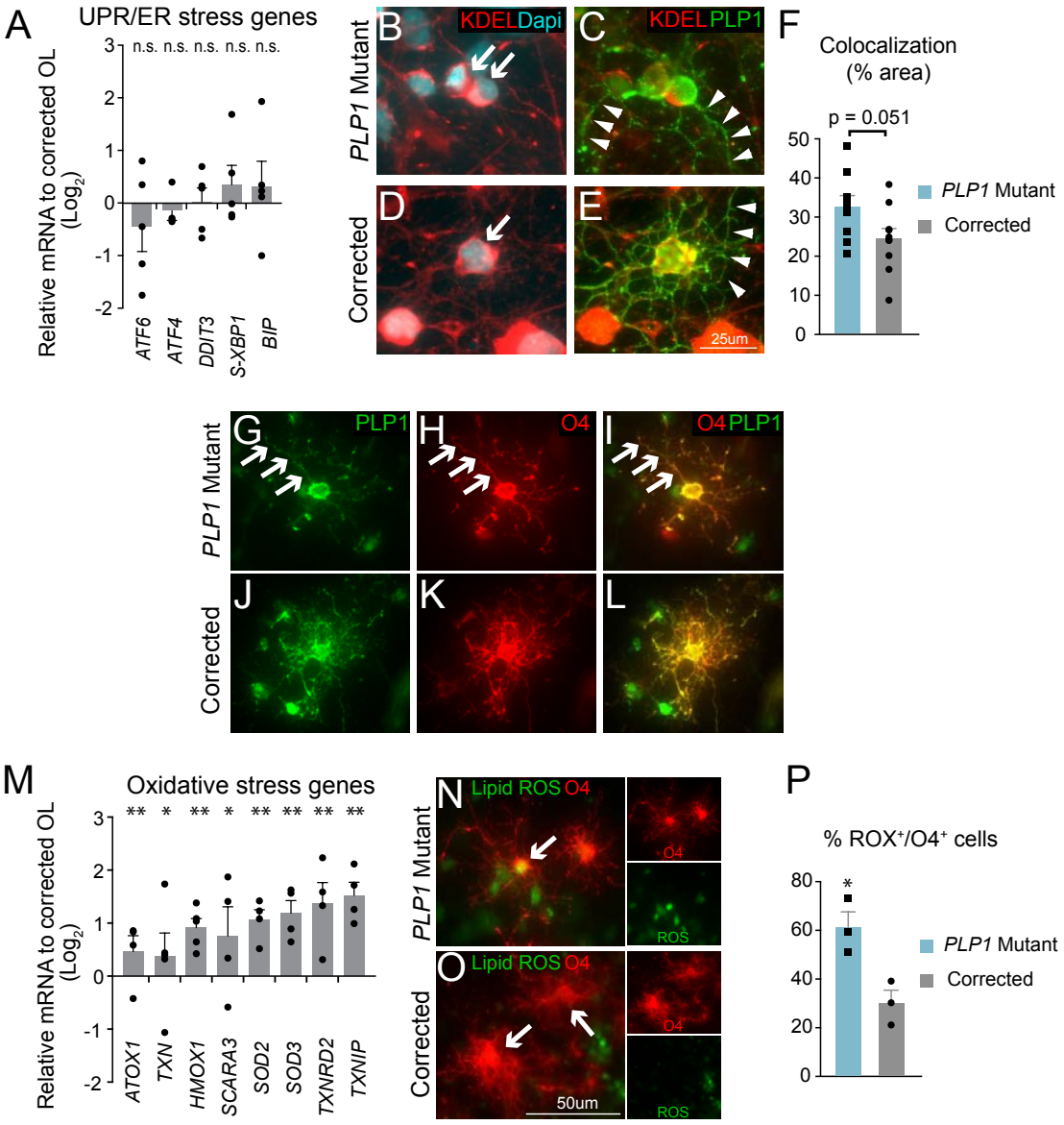
A
UPR/ER stress genes
n.s. n.s. n.s. n.s. n.s.
Relative mRNA to corrected OL (Log2)
ATF6
ATF4
DDIT3
S-XBP1
BIP
B KDELDapi
C KDEL PLP1
D
E
25um
PLP1 Mutant
Corrected
F
Colocalization (% area)
p = 0.051
PLP1 Mutant
Corrected
G PLP1
H O4
I O4 PLP1
J
K
L
M
Oxidative stress genes
** * ** * ** ** ** **
Relative mRNA to corrected OL (Log2)
ATOX1
TXN
HMOX1
SCARA3
SOD2
SOD3
TXNRD2
TXNIP
N Lipid ROS O4
O4
ROS
O Lipid ROS O4
50um
P
% ROX+/O4+ cells
PLP1 Mutant
Corrected

Figure 4

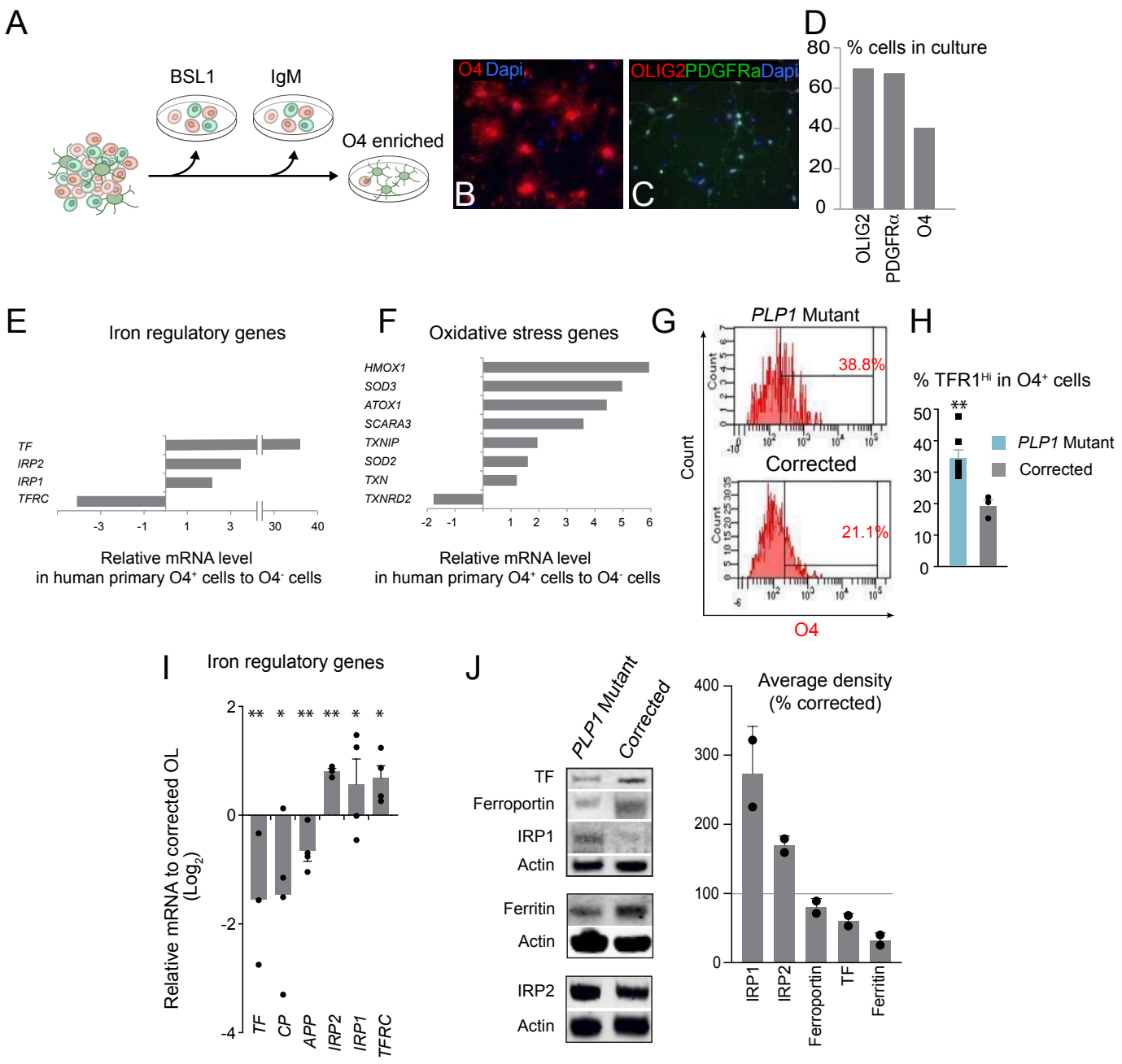
A
BSL1
IgM
O4 enriched
O4 Dapi
B
OLIG2PDGFRaDapi
C
D
% cells in culture
80
60
40
20
0
OLIG2
PDGFRα
O4
E
Iron regulatory genes
TF
IRP2
IRP1
TFRC
-3
-1
1
3
30
40
Relative mRNA level
in human primary O4+ cells to O4- cells
F
Oxidative stress genes
HMOX1
SOD3
ATOX1
SCARA3
TXNIP
SOD2
TXN
TXNRD2
-2
-1
1
2
3
4
5
6
Relative mRNA level
in human primary O4+ cells to O4- cells
G
PLP1 Mutant
38.8%
Corrected
21.1%
Count
O4
H
% TFR1Hi in O4+ cells
**
50
40
30
20
10
0
PLP1 Mutant
Corrected
I
Iron regulatory genes
Relative mRNA to corrected OL
(Log2)
2
0
-2
-4
** * ** ** * *
TF
CP
APP
IRP2
IRP1
TFRC
J
PLP1 Mutant
Corrected
TF
Ferroportin
IRP1
Actin
Ferritin
Actin
IRP2
Actin
Average density
(% corrected)
400
300
200
100
0
IRP1
IRP2
Ferroportin
TF
Ferritin

Figure 5

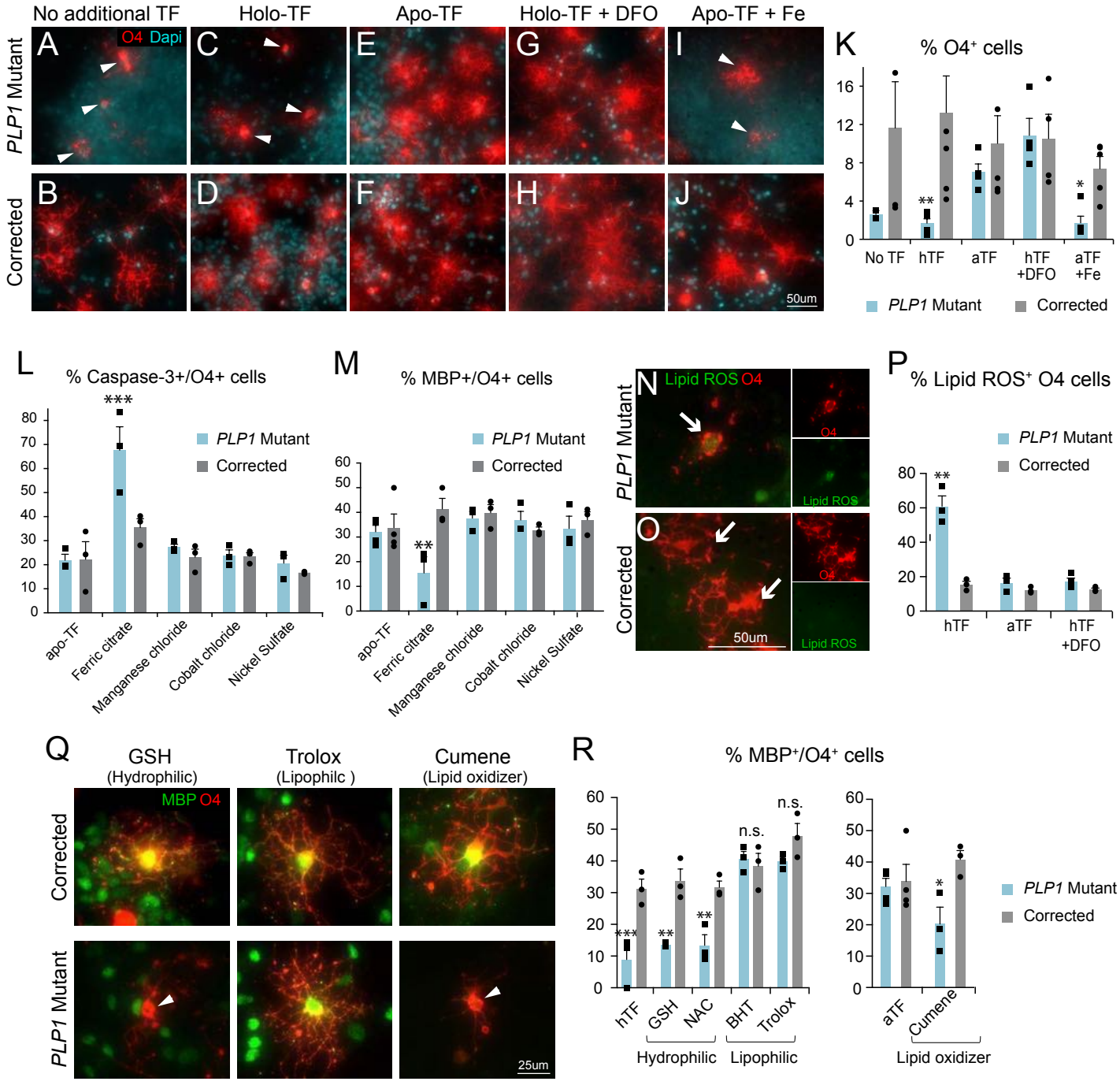
No additional TF
Holo-TF
Apo-TF
Holo-TF + DFO
Apo-TF + Fe
PLP1 Mutant
Corrected
A
O4 Dapi
B
C
D
E
F
G
H
I
J
50um
K
% O4⁺ cells
No TF
hTF
aTF
hTF +DFO
aTF +Fe
PLP1 Mutant
Corrected
L
% Caspase-3+/O4+ cells
apo-TF
Ferric citrate
Manganese chloride
Cobalt chloride
Nickel Sulfate
M
% MBP+/O4+ cells
N
Lipid ROS O4
O4
Lipid ROS
O
50um
P
% Lipid ROS⁺ O4 cells
hTF
aTF
hTF +DFO
Q
GSH
(Hydrophilic)
Trolox
(Lipophilc)
Cumene
(Lipid oxidizer)
MBP O4
25um
R
% MBP⁺/O4⁺ cells
hTF
GSH
NAC
BHT
Trolox
n.s.
Hydrophilic
Lipophilic
aTF
Cumene
Lipid oxidizer

Figure 6

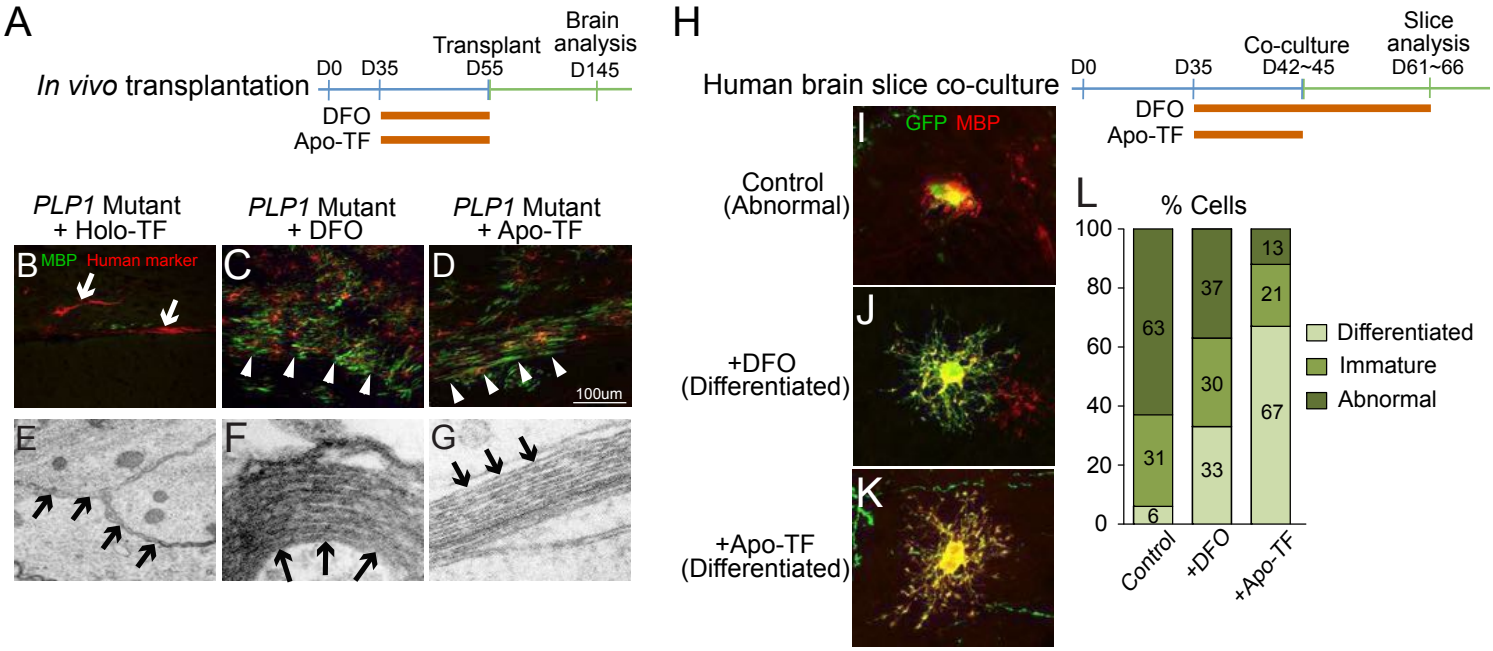
A
In vivo transplantation
D0
D35
Transplant
D55
Brain analysis
D145
DFO
Apo-TF
PLP1 Mutant + Holo-TF
PLP1 Mutant + DFO
PLP1 Mutant + Apo-TF
B
MBP
Human marker
C
D
100um
E
F
G
H
Human brain slice co-culture
D0
D35
Co-culture
D42~45
Slice analysis
D61~66
DFO
Apo-TF
Control (Abnormal)
+DFO (Differentiated)
+Apo-TF (Differentiated)
I
GFP
MBP
J
K
L
% Cells
100
80
60
40
20
0
63
31
6
37
30
33
13
21
67
Differentiated
Immature
Abnormal
Control
+DFO
+Apo-TF

Figure 7

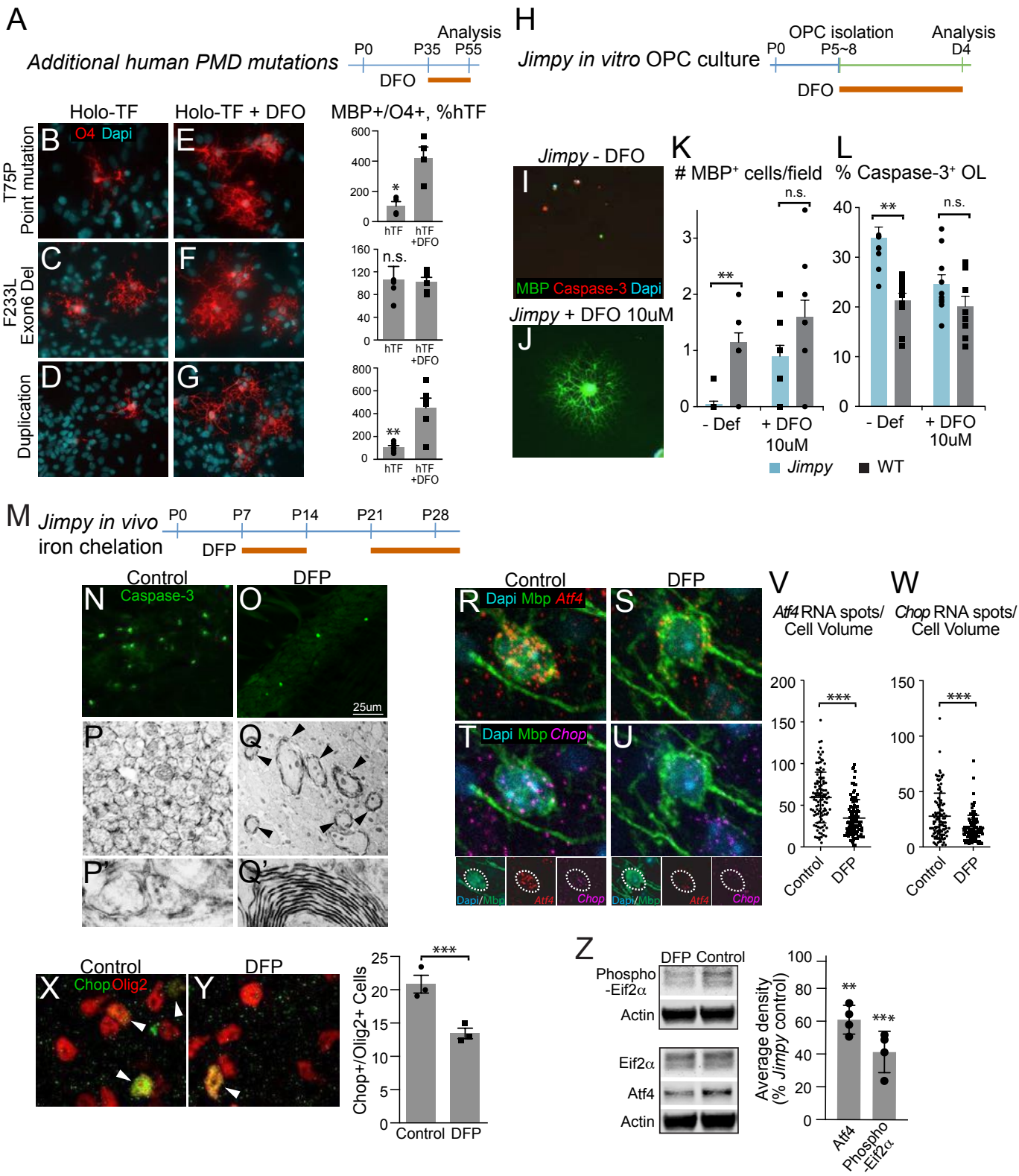
A
Additional human PMD mutations
P0
P35
P55
Analysis
DFO
Holo-TF
Holo-TF + DFO
MBP+/O4+, %hTF
T75P Point mutation
F233L Exon6 Del
Duplication
O4 Dapi
hTF
hTF +DFO
n.s.
H
Jimpy in vitro OPC culture
OPC isolation
P0
P5~8
Analysis
D4
DFO
Jimpy - DFO
MBP Caspase-3 Dapi
Jimpy + DFO 10uM
K
MBP+ cells/field
- Def
+ DFO 10uM
L
% Caspase-3+ OL
Jimpy
WT
M
Jimpy in vivo iron chelation
P0
P7
P14
P21
P28
DFP
Control
DFP
Caspase-3
25um
R
Dapi Mbp Atf4
T
Dapi Mbp Chop
V
Atf4 RNA spots/ Cell Volume
W
Chop RNA spots/ Cell Volume
X
Chop Olig2
Y
Chop+/Olig2+ Cells
Z
DFP Control
Phospho -Eif2α
Actin
Eif2α
Atf4
Average density (% Jimpy control)

Supplemental Figure 1

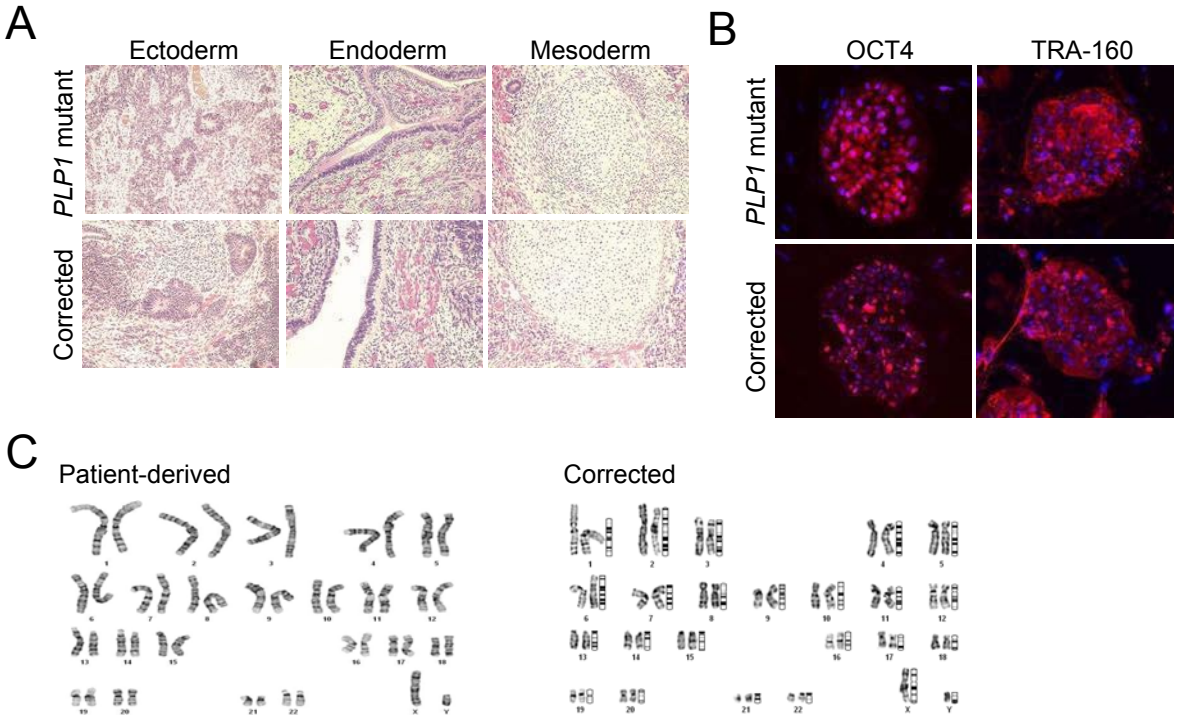

Supplemental Figure 2

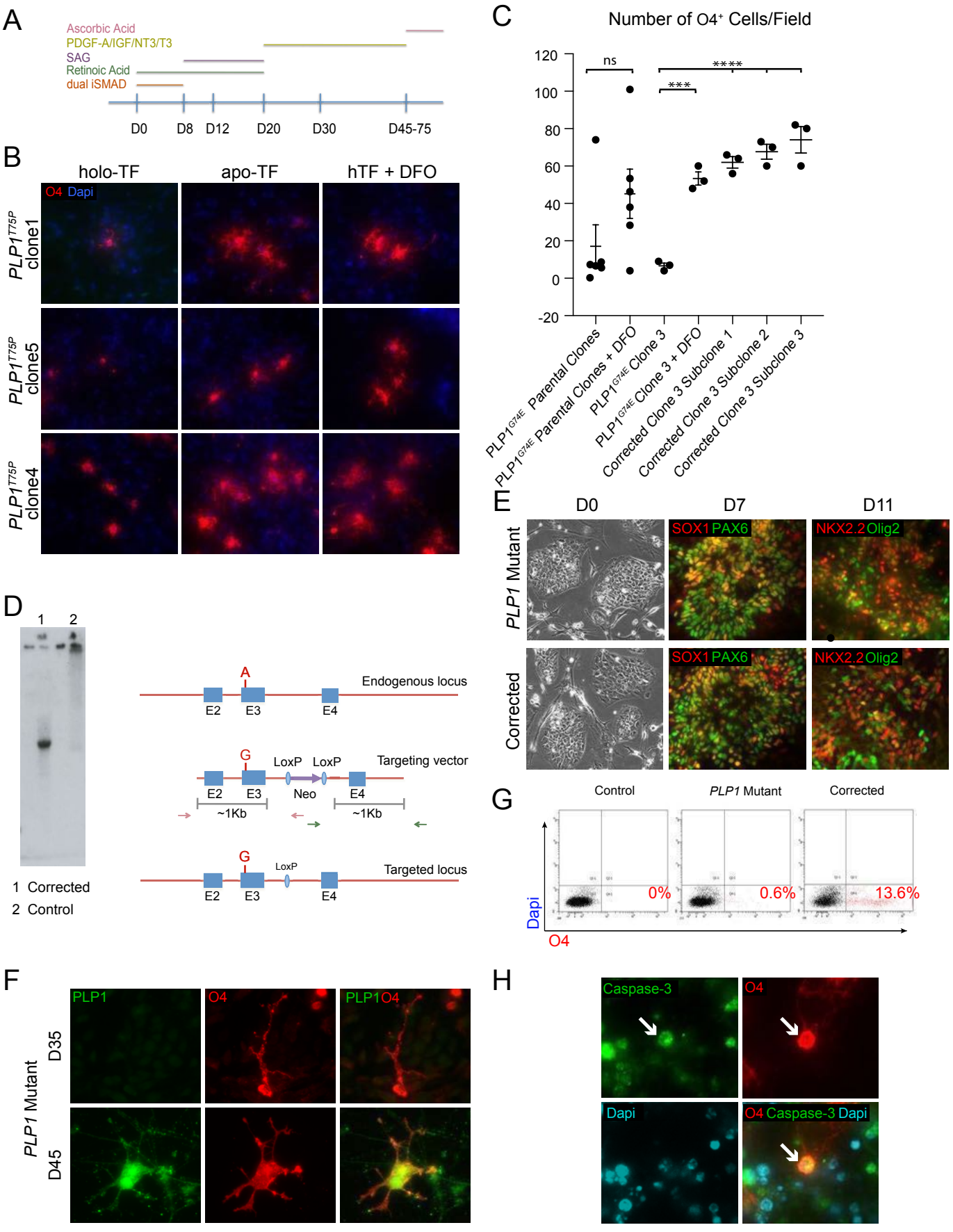

Supplementary Figure 3

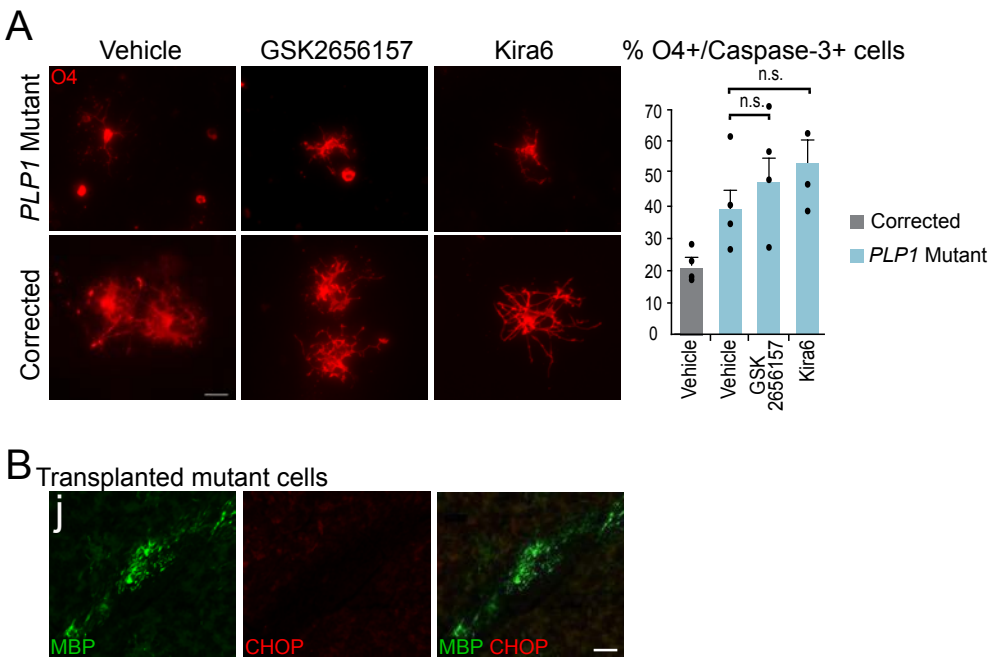

Supplementary Figure 4

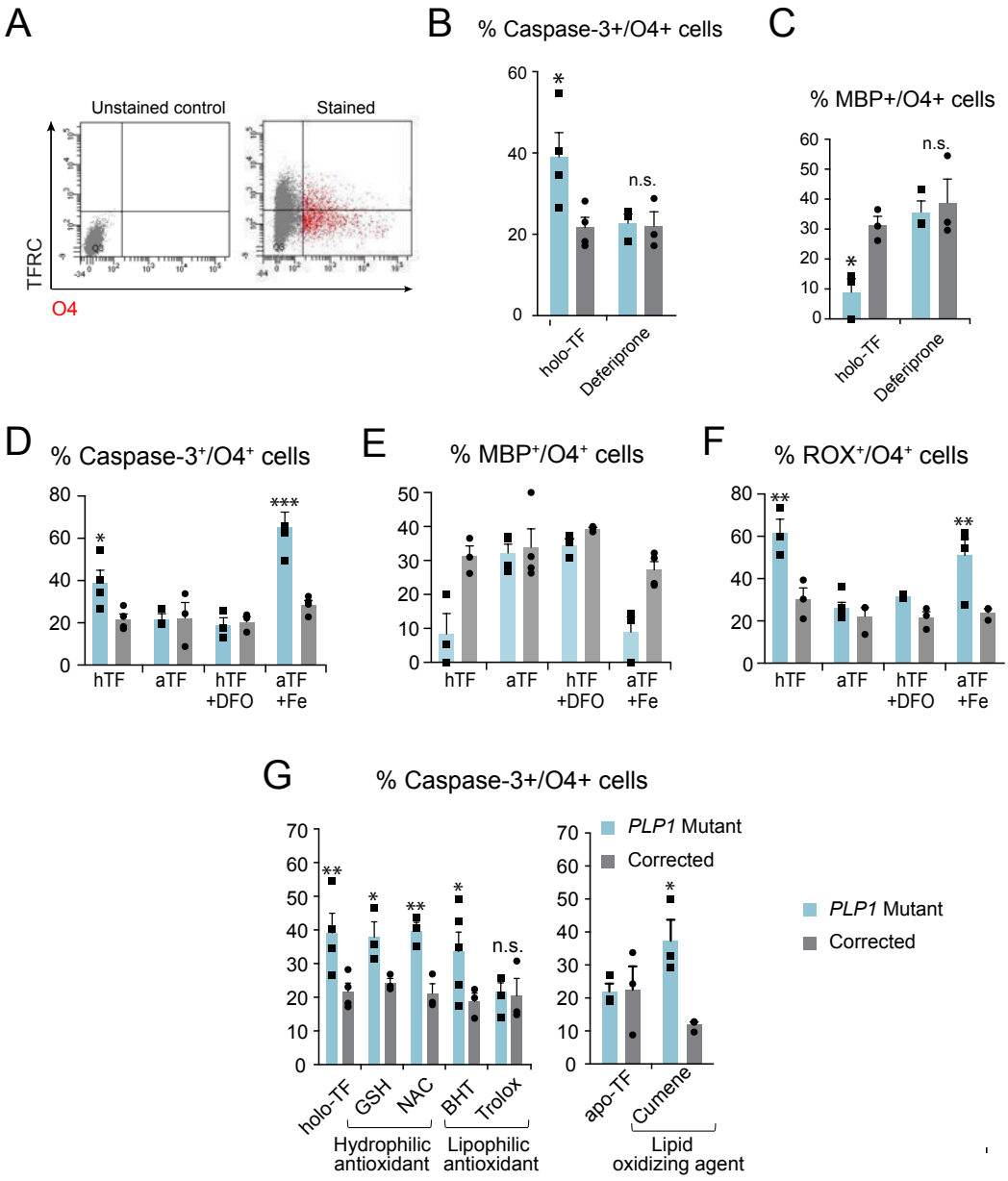

Supplemental Figure 5